MET O 11 TECHNICAL NOTE NO 119

# MESOSCALE MODELLING

by

P.W.WHITE

---

Lectures given at the ECMW Seminar on'The Interpretation and use of Large-scale Numerical Forecast Products'.
4 - 8 September 1978.

---

Meteorological Office (Met O 11)
London Road
Bracknell
Berkshire
United Kingdom

September 1978

N.B. This paper has not been published. Permission to quote from it should be obtained from the Assistant Director of the above Meteorological Office branch.

## 1. Scales of motion in the atmosphere

It is conventional to classify atmospheric phenomena according to their characteristic scales and, for convenience, the spectrum is usually divided into five parts:- planetary scale, synoptic scale, mesoscale and microscale (Fig.1)

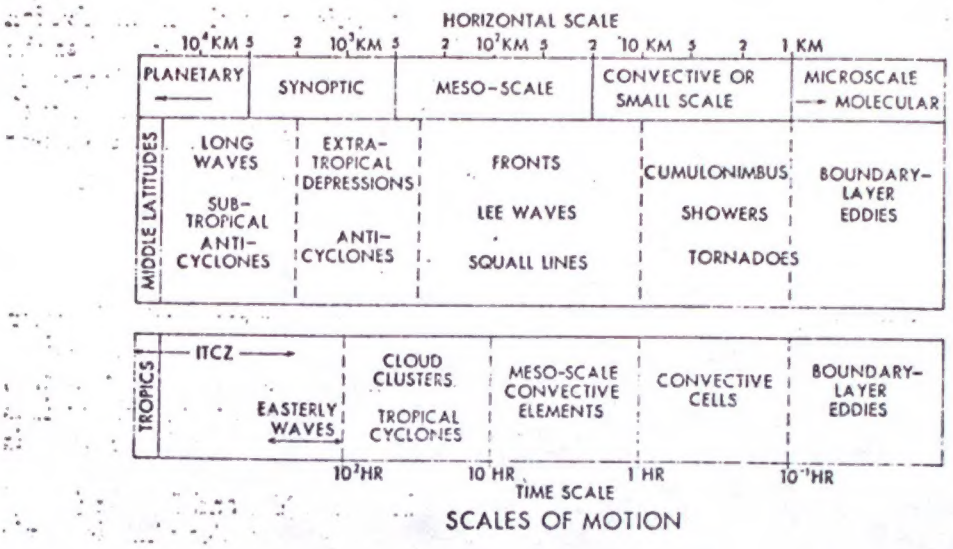


**Fig. 1**

For many years numerical models have been used with considerable success for predicting the behavious of phenomena in the planetary and synoptic scales, while the important mechanisms for heat, moisture and momentum transfer on the small and microscales have been represented in these models by parameterisation schemes.

The mesoscale region has, until recent years, been somewhat neglected by numerical modellers. For the most part, studies of this region of wavenumber space have been made using simplified analytic models or numerical integrations of idealised situations. Only in the past few years has work started on the problem of real data simulations. Furthermore, there is still only a sketchy understanding of the ways in which the mesoscale controls or interacts with larger and smaller scales. The problem of parameterisation has been tacitly ignored by modellers who put their faith in diffusion schemes with coefficients determined by rather tenuous arguments concerning the maintenance of the energy spectrum. Practical forecasters, however, have always been concerned with the mesoscale, since it is primarily on this scale that forecasts are required.

The increasing interest in mesoscale dynamics stems from two sources, the numerical modeller who requires better parameterisation schemes and the forecaster who wishes to predict the local weather. A further aspect of interest, which may receive greater attention in the future, is that of local climatology and its dependence on man's industrial and agricultural activities.

It is instructive to put the classification shown in Fig. 1 on a more theoretical footing. We can show, using simplified sets of equations, that the different regions of the spectrum are dynamically distinct. Let us consider the following equation describing the dynamics of small amplitude perturbations of a hydrostatic incompressible atmosphere.

$$\frac{\partial u'}{\partial t} + U\frac{\partial u'}{\partial x} - f v' + c_p \theta_0 \frac{\partial p'}{\partial x} = 0 \qquad (1)$$

$$\frac{\partial v'}{\partial t} + U\frac{\partial v'}{\partial x} + f u' + c_p \theta_0 \frac{\partial p'}{\partial y} = 0 \qquad (2)$$

$$-g\frac{\theta'}{\theta_0} + c_p \theta_0 \frac{\partial p'}{\partial z} = 0 \qquad (3)$$

$$\frac{\partial \theta'}{\partial t} + U\frac{\partial \theta'}{\partial x} + w'\frac{d\theta_0}{dz} = 0 \qquad (4)$$

$$\frac{\partial u'}{\partial x} + \frac{\partial v'}{\partial y} + \frac{\partial w'}{\partial z} = 0 \qquad (5)$$

In these equations U is a basic wind in the x direction, (u', v', w') are the components of the perturbed wind in the (x,y,z) directions, P' is proportional to the perturbed pressure, $\theta_0$ is the potential temperature of the basic atmosphere and $\theta'$ is the perturbation potential temperature. Since we are not concerned with planetary scales we regard the gravitational acceleration g and the Coriolis parameter f as constants and, $\theta_0$ is taken as constant except where it is differentiated with respect to z, when $d\theta_0/dz$ is taken as constant. We may easily show that wave solutions of the form

$$\begin{bmatrix} u' \\ v' \\ w' \\ \theta' \\ p' \end{bmatrix} \propto \exp\left[i(kx + ly + mz - \omega t)\right]$$

are possible provided that the following dispersion relationship exists between the frequency $\omega$, the two horizontal wave numbers (k,l) and the vertical wave number m

$$(\omega - kU)\left[(\omega - kU)^2 - \{f^2 + N^2(k^2+l^2)/m^2\}\right] \qquad (6)$$

where N is the Brunt Vaissala frequency defined by $N^2 = g\,\theta_0^{-1}\, d\theta_0/dz$ This equation has three solutions, one corresponding to simple advection (this would have taken the form of a dispersion relation for the conventional Rossby wave if we had allowed f to vary) and the other two corresponding to inertial gravity waves. Rearranging (6) gives an expression for the vertical wavenumber m

$$m^2 = \frac{N^2(k^2+l^2)}{(\omega - kU)^2 - f^2}$$

Clearly the vertical phase velocity $\omega/m$ and group velocity $\partial\omega/\partial m$ are only non zero if m is real (when m is imaginary the waves propagate only horizontally and the vertical structure is exponential in z rather than sinusoidal), which implies that the frequency relative to the flow $(\omega - kU)$ must be greater than f (i.e. the waves must have periods less than $2\pi/f \approx$ 15 hours in mid latitudes). Waves stationary relative to the ground (such as steady state lee waves set up as a result of airflow over a mountain) actually travel upstream relative to the air with a horizontal phase speed of $-U$. Hence $\omega \equiv 0$ and we deduce that these waves also have a vertical component of propagation unless their horizontal wavelength is greater than $2\pi U/f$. For $U = 10$m/sec and $f = 10^{-4}$sec$^{-1}$ this corresponds to about 600km.

This discussion can be generalised to include non-hydrostatic vertical accelerations in the system of equations. Equation ( 3 ) is then replaced by

$$\frac{\partial w'}{\partial t} + U\frac{\partial w'}{\partial x} - g\frac{\theta'}{\theta_0} + c_p\theta_0\frac{\partial p'}{\partial z} = 0 \qquad (7)$$

and the dispersion relationship ( 6 ) becomes

$$(\omega - kU)\left[(\omega - kU)^2 - \left\{f^2 m^2 + N^2(k^2+l^2)\right\}\right]/(k^2+l^2+m^2) \qquad (8)$$

Then, for a stationary wave system ( $\omega = 0$ ), the vertical wavenumber m is given by

$$m^2 = (k^2+l^2)(N^2 - U^2k^2)/(k^2U^2 - f^2)$$

which indicates that, for a vertical component of propagation to be possible, the horizontal wavelength must not only be less than $2\pi U/f$ but also be greater than $2\pi U/N$ . For $U = 10\text{msec}^{-1}$ and $N = 10^{-2}\text{sec}^{-1}$ this second limiting scale corresponds to about 6km.

The range of scales 6 - 600km, in which a vertical component of propagation arises for waves which are stationary with respect to the ground, corresponds closely to the interval in the spectrum which we identify on observational grounds as the meso-scale. While the precise values of the limits of this spectral band obviously depend on the prevailing atmospheric conditions, the analysis strongly suggests that the mesoscale is characterised by a general transmission of information about disturbances to the flow at the earth's surface into the main body of the atmosphere. The theory presented here is, of course, highly idealised and does not imply that upward propagation of gravity wave energy is impossible outside this region of the spectrum (it may arise, for example, in unsteady flow over a mountain range), nor even that mesoscale gravity wave activity is more intense than at other scales, but it does lend some support to the idea that the neglect of the influence of the mesoscale on larger scales in numerical weather prediction models may be a serious defect.

When compressibility is included into the system, the continuity equation ( 5 ) takes the form

$$\frac{\partial \rho'}{\partial t} + U\frac{\partial \rho'}{\partial x} + w'\frac{d\rho_0}{dz} + \rho_0\left(\frac{\partial u'}{\partial x} + \frac{\partial v'}{\partial y} + \frac{\partial w'}{\partial z}\right) = 0 \qquad (9)$$

where $\rho_0$ is the density of the basic atmosphere and $\rho'$ is the perturbation density (related to $\theta'$ and $p'$ by the equation of state). There is then some modification to the gravity waves (principally due to the term $w\,d\rho_0/dz$ ), but the most marked alteration to the wave dispersion equation is the introduction of an additional set of waves with

much higher frequencies:- acoustic waves. As with gravity waves, acoustic waves are subject to conditions which govern whether they propagate internally along rays inclined to the horizontal or purely horizontally. A special kind of horizontally propagating wave is the Lamb wave which is subject to the constraint $\partial(w\rho_0)/\partial z=0$ (which leaves ( 9 ) as essentially a two dimensional equation) and whose frequency is given by $\omega^2=k^2c^2+f^2$ , where c is the speed of sound.

It is well known to synoptic scale modellers that high frequency acoustic waves do not arise in a hydrostatic compressible system, but the Lamb wave remains (in a hydrostatic model it is often referred to as the external gravity wave). Much fuller discussions of atmospheric waves is given in the literature (e.g. Eckart (1960)), but the essentials of the above discussion are given in Fig. 2.

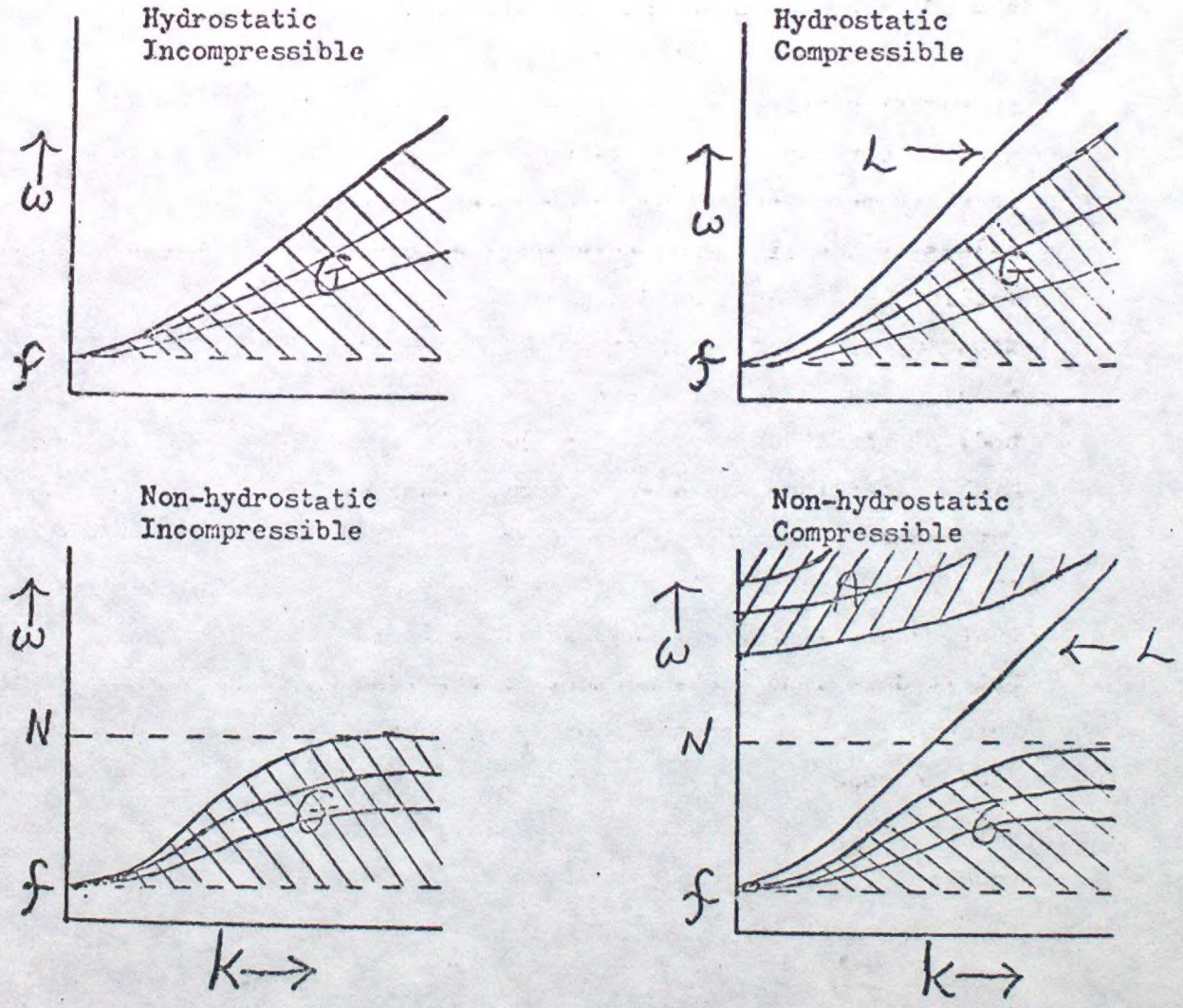


Fig. 2.

Schematic frequency diagrams for different approximations A=acoustic, L=Lamb, G=gravity wave regions.

## 2. Analytic modelling

A rigorous analytic study of mesoscale phenomena is very difficult and has only been successful for a limited number of simplified cases. However, a general discussion of the kind of dynamics controlling the development of certain features is often instructive in indicating their character even though it may not be universely applicable. In this section we consider a number of such examples.

### a) Frontogenesis.

Hoskins (1971) pointed out the importance of ageostrophic advection in rapid frontogenesis in the presence of a deformation field. He distinguished between the quasi-geostrophic equations

$$\frac{\partial \underline{v}_g}{\partial t} + \underline{v}_g \cdot \nabla \underline{v}_g + f\, \underline{k} \times \underline{v} + \nabla \phi = 0$$

$$\underline{v}_g = \frac{1}{f}\, \underline{k} \times \nabla \phi$$

and the semi-geostrophic equations

$$\frac{\partial \underline{v}_g}{\partial t} + \underline{v} \cdot \nabla \underline{v}_g + f\, \underline{k} \times \underline{v} + \nabla \phi = 0$$

(in the quasi-geostrophic equations only advection by the geostrophic wind is considered).

The different dynamical character of these equations can be illustrated by the corresponding gradient wind equations for steady flow along curved trajectories of radius r. The full equations give the gradient wind equation

$$\frac{v^2}{r} + fv = f v_g$$

while for the quasi-geostrophic and semi-geostrophic equations we have

$$\frac{v_g^2}{r} + fv = f v_g$$

$$\frac{v v_g}{r} + fv = f v_g$$

respectively. Introducing the two Rossby numbers $R = 2v/fr$ and $R_g = 2v_g/fr$, the three equations become

$$R = -1 + (1 + 2R_g)^{1/2}$$

$$R = R_g (1 - R_g/2)$$

$$R = R_g / (1 + R_g/2)$$

The relationship between R and $R_g$ is illustrated in Fig. 3, and we can see the improvement in accuracy of the semi-geostrophic over the quasi-geostrophic system (the latter is particularly inaccurate for $R_g > 1$ ).

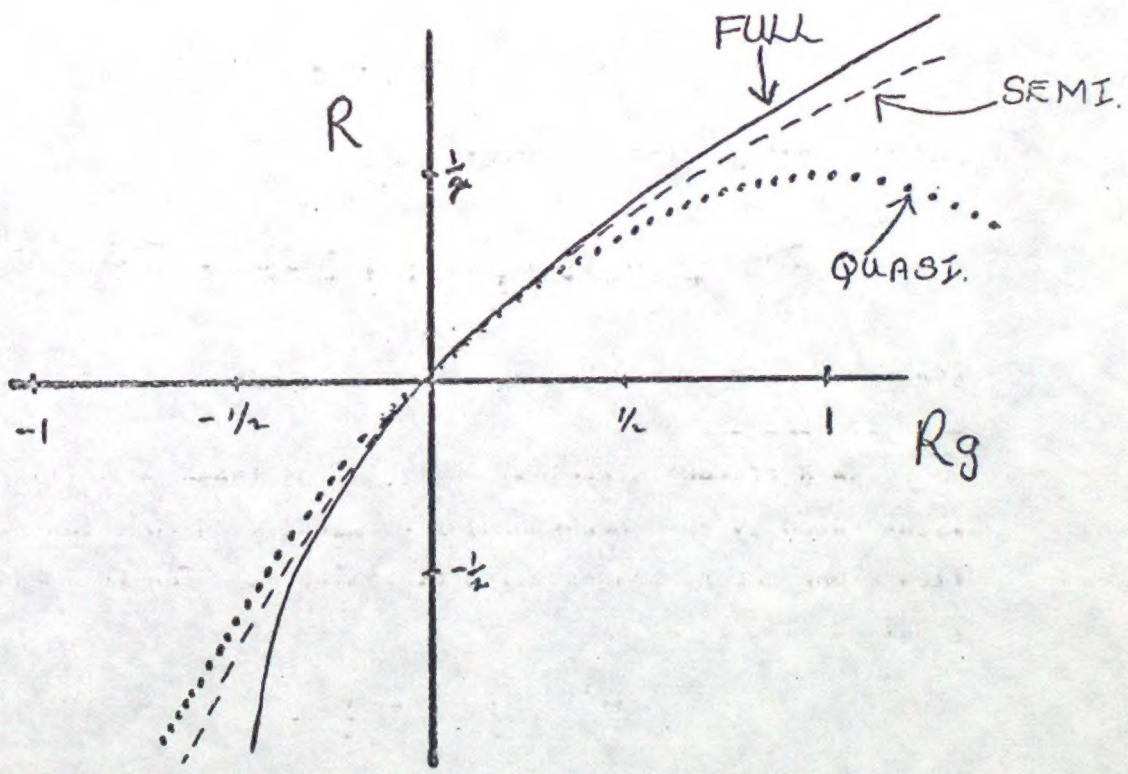


Fig. 3

In considering frontal development, we imagine a pre-existing weak concentration of temperature gradient embedded in a large scale deformation field given by $u = -\gamma x$ , $v = \gamma y$ (see Fig.4)

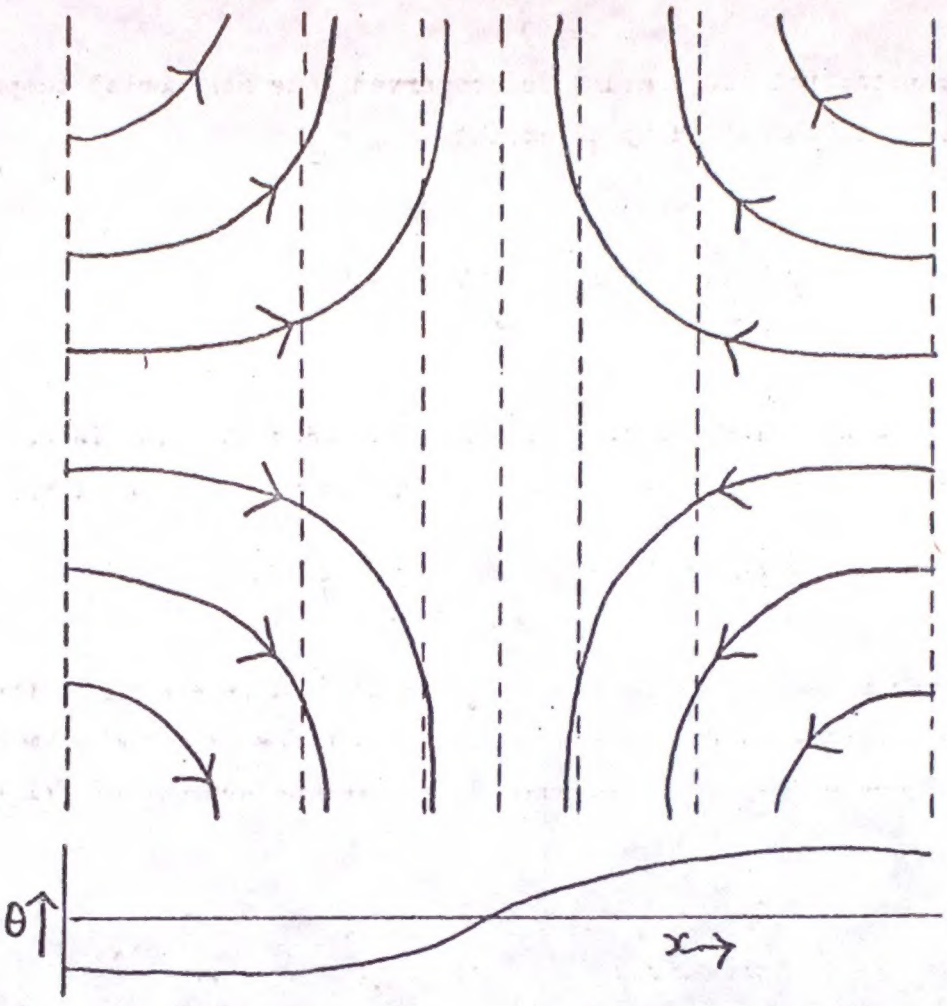


Fig. 4.

Winds in the y direction (i.e. along the incipient from) are regarded as being geostrophic while in the x direction ageostrophic winds can occur.

A fluid element will be deformed in both the x and y directions. Concentrating on the x axis the length L of the element will become $L + \delta L$ after a time $\delta t$ , where $\delta L = -\gamma L \delta t$

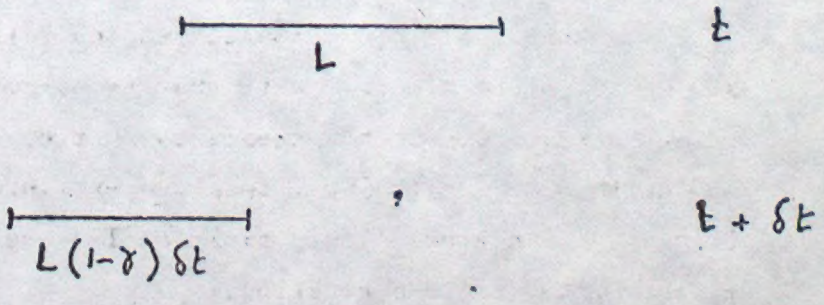


If $\gamma$ were constant in time this would lead to an exponential decay $L = L_0 e^{-\gamma t}$ so that L would shrink to zero after an infinite time.

Since potential temperature is conserved, the horizontal temperature gradient is increased by an amount

$$\delta\left(\frac{\partial\theta}{\partial x}\right) = \frac{\partial\theta}{\partial x}\,\gamma\,\delta t$$

Because winds in the y direction are regarded as being in geostrophic balance, the thermal wind equation implies a change in $\partial v_g/\partial z$

$$\delta\left(\frac{\partial v_g}{\partial z}\right) = \frac{\partial\theta}{\partial x}\,\frac{g}{f\theta_0}\,\gamma\,\delta t$$

From the equations of motion, $Dv_g/Dt = -fu_a$ (where $u_a$ is the ageostrophic wind in the x direction), but the mean momentum of the atmosphere of depth H is unaffected (in the absence of friction) so that

$$\frac{D}{Dt}\left(\frac{\partial v_g}{\partial z}\right) \approx -\frac{2}{H}\,\frac{Dv_g}{Dt} = \frac{2f}{H}\,u_a$$

at ground level. Thus an ageostrophic wind is generated in the positive x direction with a magnitude proportional to the initial temperature gradient. Because the initial value of the horizontal temperature gradient has a maximum at the origin and decays to zero at $x = \pm\infty$, $\partial u_a/\partial x < 0$, i.e. the secondary flow strengthens the basic deformation. The fluid element length thus decays faster than $e^{-\gamma t}$ and Hoskins (1971) showed that a discontinuity is formed in a finite time. If the quasi-geostrophic equations were used an ageostrophic component $u_a$ would still arise but there would be no feedback into the advection and the discontinuity would take an infinite time to form.

b) Sea Breezes.

Simpson (1969) has compared mesoscale flows, such as sea breezes and thunderstorm outflows, with gravity currents induced in Laboratory water tanks. Consider a steady current of fluid with a density $\rho+\Delta\rho$ and depth $d$ flowing into a deeper fluid of depth H and density $\rho$ (Fig.5). Since relatively small scales are involved we neglect the effect of the earth's rotation.

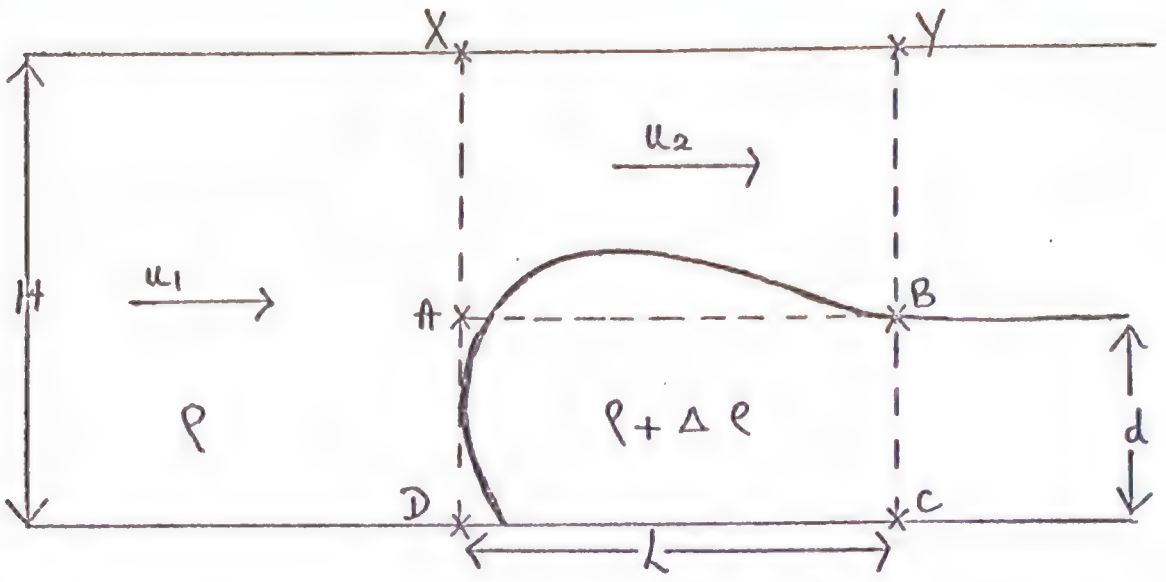


Fig. 5.

Using a coordinate system moving relative to the denser fluid, the mean pressures across AD and BC must be equal in the absence of friction. If the density and vertical pressure gradients are related hydrostatically

$$2 P_A + \rho g d = 2 P_B + (\rho + \Delta\rho) g d$$

Using Bernoulli's theorem

$$\tfrac{1}{2} \rho u_1^2 + P_A = \tfrac{1}{2} \rho u_2^2 + P_B$$

and the continuity equation

$$u_1 H = u_2 (H - d)$$

and eliminating $P_A$ and $P_B$ we obtain an expression for $u_1$ (the speed of propagation of the denser fluid current into a

stationary lighter fluid)

$$u_1^2 = g \frac{\Delta\rho}{\rho} \frac{(H-d)^2}{2H-d} \qquad (10)$$

Alternatively we can consider the momentum budget of the entire region XYCD. Evidently

$$\frac{\partial}{\partial x}\left[ \int \rho u^2 dz + \int p\, dz \right] = 0$$

for steady frictionless flow. Using Bernouilli's theorem and the continuity equation gives

$$u_1^2 = g \frac{\Delta\rho}{\rho} \frac{(H-d)^2}{H}$$

This is different to ( 10 ). Benjamin (1968) pointed out that this discrepancy implies that steady flow can only arise if dissipation is present. Simpson et al (1977) recalculated an expression for $u_1$ assuming that stresses $\tau_t$ and $\tau_b$ act at the top and bottom of the denser fluid over a distance L at the head of the gravity current. They then obtained

$$u_1^2 = \left[ g \frac{\Delta\rho}{\rho} - \frac{2L}{d^2}\left( \tau_b + \tau_t \frac{H}{H-d} \right) \right] \frac{(H-d)^2}{2H-d}$$

By substituting values measured during an actual sea breeze near the south coast of England on the 14th June 1973 they concluded that the drag at the top of the denser fluid was about five times as large as the drag at the surface. This is confirmed qualitatively by laboratory experiments which show an appreciable amount of mixing at the head of the gravity current, and by glider pilots who have reported strong turbulence in this region even after general convection has ceased. (Fig.6)

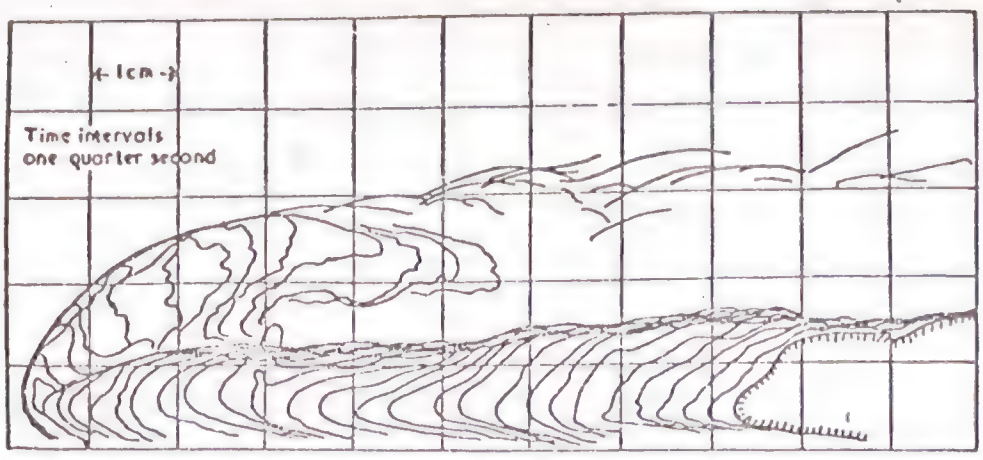


Flow pattern inside a laboratory gravity current head, showing successive positions of a dye patch inserted in the dense fluid moving towards the head.

(Simpson, Mansfield and Milford (1977))

Fig. 6

c) Convective storms.

Green and Moncrieff (1972) and more recently Moncrieff (1978) discussed the dynamics of a steady state convective storm in sheared flow. They considered two dimensional over turning of the sort illustrated in Figs. 7a and 7b.

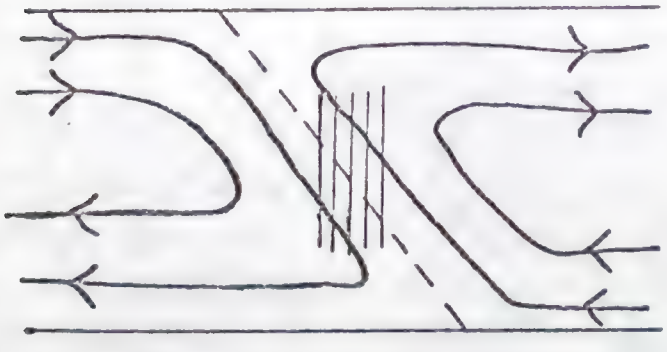

Fig.7a

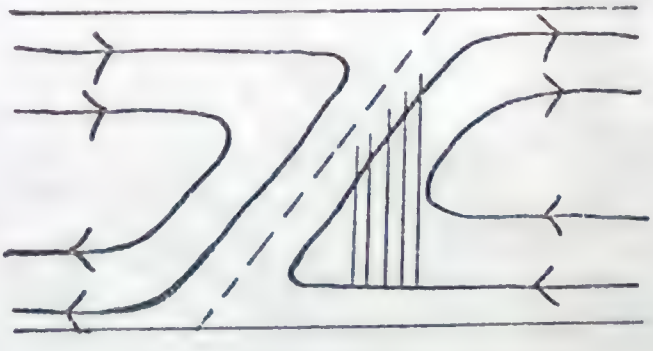

Fig. 7b.

The structure in Fig 7a is consistent with the case study of Browning and Ludlam (1962) and permits rain formed in the updraft to evaporate in the downdraft. The analytic description of these systems is based on the horizontal components of the vorticity equation

$$\frac{D}{Dt}\left(\frac{\partial u}{\partial z} - \frac{\partial w}{\partial x}\right) + \frac{g}{\theta_0}\frac{\partial \theta}{\partial x} = 0 \qquad (11)$$

where the incompressibility assumption has been made (this is not essential but the neglect of compressibility simplifies the present discussion).

If $\psi$ is a stream function defined by $u = \partial\psi/\partial z$ and $w = -\partial\psi/\partial x$ we can transform from $(x, z)$ to $(\psi, z)$ coordinates and consider the Lagrangian form of equation (11 ). Assuming that the inflow parameters are given and also that the rate at which the potential temperature of an air parcel changes along a trajectory is known, (including the effect of latent heat release) the equation can be reduced to a conservative form. For the simplest case where values of these input parameters are constant, the vorticity equation may be integrated along a trajectory to give

$$\nabla^2\psi = 1 + R\,(z - z_0)/(z_* - z_0)$$

where R is the ratio of the convective available potential energy to the change in kinetic energy along a streamline, $z_0(\psi)$ is the inflow height and $z_*$ is the steering level. When R is positive, potential energy is converted in to kinetic energy, but when R is negative the storm acquires energy from the mean flow.

Solution of this equation, with suitable boundary conditions implying continuity of pressure across the interface between the up and downdraft, leads to a determination of conditions on the outflow, the height of the steering level and the nature of the interface between the up and downdraft.

Several points of interest arise. Firstly solutions only exist for $-\frac{1}{4} \leq R \leq 1$ . Negative values of R correspond to a structure similar to Fig.7a (with the updraft lying above the downdraft) while for positive values the orientation of the interface is reversed as in Fig.7b. (a structure that is apparently not observed in the atmosphere and does not permit evaporation of rain in the downdraft). Since a negative value of R implies forced convection, a storm with structure shown in Fig.7a can only be transient. We are thus lead to the conclusion that steady convective storms must have a three dimensional structure for the thermodynamics of the condensation and evaporation to fit consistently with the dynamical constraints.

The above dynamical description is non hydrostatic. If the hydrostatic assumption is made the maximum vertical velocities are related approximately to those in the non hydrostatic model by

$$w(\text{hydrostatic}) \approx \left(\frac{R+1}{R+1/2}\right)^{1/2} w(\text{non-hydrostatic})$$

Thus larger vertical velocities are produced in a hydrostatic model (about 40% larger for R=$\frac{1}{4}$ and 13% for R=1). This feature of greater instability of hydrostatic models can also be deduced from equations ( 6 ) and ( 8 ) which neglecting the Coriolis parameter become $\omega^2 = N^2(k^2+l^2)/m^2$ for a hydrostatic atmosphere and $\omega^2 = N^2(k^2+l^2)/(k^2+l^2+$ for a non-hydrostatic model. If the lapse rate is unstable ($N^2 < 0$) then perturbation grows like exp ( $\sigma t$ ) where

$$\sigma^2 = |N^2|(k^2+l^2)/m^2 \qquad \text{(hydrostatic)}$$

$$\sigma^2 = |N^2|(k^2+l^2)/(k^2+l^2+m^2) \qquad \text{(non-hydrostatic)}$$

Clearly $\sigma^2$(hydrostatic) $> \sigma^2$(non-hydrostatic) and we deduce an important characteristic of hydrostatic models, namely that they are more sensitive to convective instability than non-hydrostatic models.

d) Mountain blocking.

When an airflow interacts with orography, it may flow over the mountain, around it or a combination of both. If the mountain barrier is sufficiently long, blocking of the airstream may arise, in which case the blocked air can be diverted substantially from its original course, even to the extent of being forced to return upstream thereby causing modifications to the flow far upstream. (Fig.8). Such behaviour may be one way in which a relatively narrow mountain range might substantially affect the synoptic scale flow.

We can estimate whether blocking is likely to arise by examining the energy of the air approaching the mountain (Eliassen 1973)

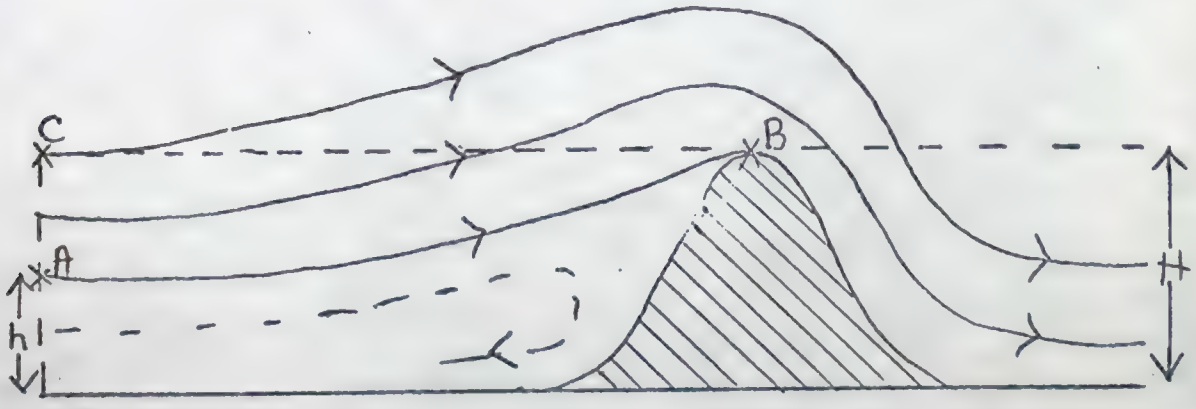


Fig. 8

Assuming a steady state flow of the form shown in Fig.8 we examine the energy of the air flowing through point A along the lowest stream line to successfully cross the barrier. Using Bernoulli's theorem in a form applicable to steady adiabatic flow

$$\tfrac{1}{2} v_A^2 + g h + c_p T_A = \tfrac{1}{2} v_B^2 + g H + c_p T_B$$

The condition for the flow to cross the mountain top is $v_B^2 \geq 0$

Then

$$\tfrac{1}{2} v_A^2 \geq g(H-h) + c_p (T_B - T_A)$$

Since $\theta_A = \theta_B$

we must have

$$T_B = \theta_B \left(\frac{p_B}{1000}\right)^K = \theta_A \left(\frac{p_B}{1000}\right)^K$$

and also

$$T_A = \theta_A \left(\frac{p_A}{1000}\right)^K$$

where $k = R/c_p$ .

$$\tfrac{1}{2} v_A^2 \geq g(H-h) - c_p \theta(h) \left[\left(\frac{p(h)}{1000}\right)^K - \left(\frac{p(H)}{1000}\right)^K\right]$$

$$= c_p \int_h^H \left[\left(\frac{p(z)}{1000}\right)^K - \left(\frac{p(H)}{1000}\right)^K\right] \frac{d\theta}{dz}\, dz$$

$$= \frac{c_p}{g} \int_h^H \left[T(z) - T(H) \frac{\theta(z)}{\theta(H)}\right] N^2(z)\, dz$$

We may therefore determine if an air parcel at a given level has sufficient kinetic energy to get over the mountain, by calculating a function of the thermodynamic properties of the column of air above it.

e) Gravity waves.

Some of the effects of making the hydrostatic approximation can be examined by considering the behaviour of gravity waves. Using a coordinate system moving with the mean flow and ignoring the effect of the earth's rotation, the frequencies of two dimensional gravity waves in a hydrostatic and non hydrostatic atmosphere may be written

| Hydrostatic | Non-hydrostatic |
|---|---|
| $\omega^2 = \frac{N^2 k^2}{m^2}$ | $\omega^2 = \frac{N^2 k^2}{(k^2 + m^2)}$ |

where k is the horizontal wavenumber and me is the vertical wavenumber. The direction of the phase velocity is at right angles to the phase lines, i.e. in the direction of the vector (k,m), and its amplitude is $\omega / (k^2 + m^2)^{1/2}$. Thus

$$\underline{c} = \frac{Nk}{m} \frac{1}{k^2+m^2} (k, m) \qquad \underline{c} = \frac{Nk}{(k^2+m^2)^{3/2}} (k, m)$$

The group velocity $\underline{c}_g$ has x and z components $(\partial\omega/\partial k , \partial\omega/\partial m)$

$$\underline{c}_g = \frac{Nk}{m} \left( \frac{1}{k} , -\frac{1}{m} \right) \qquad \underline{c}_g = \frac{Nkm^2}{(k^2+m^2)^{3/2}} \left( \frac{1}{k} , -\frac{1}{m} \right)$$

We deduce that $\underline{c} . \underline{c}_g = 0$ in both hydrostatic and non-hydrostatic atmospheres, i.e. the phase and group velocities are at right angles to one another.

In the case of a stationary gravity wave train set off by a flow of speed U over a mountain, the horizontal phase speed $\omega/k$ is equal to -U and the horizontal group velocity relative to a fixed co-ordinate system is given by

$$c_{gx} = 0 \qquad c_{gx} = \frac{k^2 U^3}{N^2}$$

Since the energy of a group of waves moves with the group velocity, we see that in a hydrostatic model the wave energy stays in the vicinity of the mountain, but spreads downstream in a non-hydrostatic model.

It may be shown that if there is a downward flux of wave momentum (corresponding to a wave drag force imposed on the air by the mountain) there must also be an upward flux of wave energy. We can easily see that this implies an upstream slope of the phase lines (Fig.9).

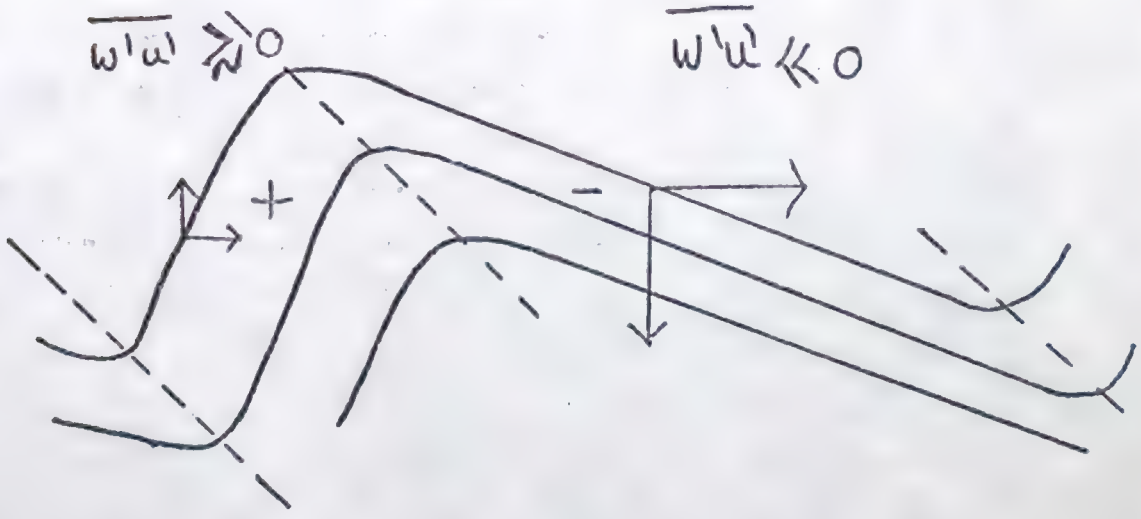


Fig. 9

The air in the ascending portion of the wave is moving more slowly than in the descending part. Hence $\overline{w'w'} < 0$. Furthermore from Bernoulli's theorem there is a positive pressure anomaly in the ascending part and a negative pressure anomaly in the descending region. The air below a given stream line exerts a force in the upstream direction on the air above and therefore does work on it as it streams through the stationary wave pattern. From the expressions for the phase and group velocity we see that an upward group velocity corresponds to a downward phase velocity.

If there is a level at which the wind speed drops to zero, the wave energy of a group of gravity waves is trapped below it. Without going into the mathematical details we can see when how and why this happens by considering the geometry of a stationary wave train. As the system moves up into a region of decreasing U the wavenumbers satisfy the following conditions locally

$$U = \frac{N}{m} \qquad\qquad U = \frac{N}{(k^2+m^2)^{1/2}}$$

In both the hydrostatic and the non hydrostatic cases the vertical wavenumber increases with decreasing U if the horizontal wave number is independent of height. Also, in both cases, the vertical group velocity tends to zero as $U \to 0$. A rigorous mathematical treatment (Booker & Bretherton '67) shows that the wave energy flux has a discontinuity, at the level U = 0. Since $m \to \infty$ as $U \to 0$, the closeness of the phase lines near the critical level ( $m \gg 0$ ) suggests a region of turbulence, though some theoretical results indicate that the wave energy is transferred to the mean flow at this level. Evidently the above argument indicates that the behaviour of waves at critical levels can be described satisfactorily by both hydrostatic and non hydrostatic models.

Another form of wave trapping arises when the wind increases or the static stability decreases with height. The vertical wavenumber m satisfies the following relationship for a stationary wave train.

$$m = l_s \qquad\qquad m = \left(l_s^2 - k^2\right)^{1/2}$$

The parameter $l_s = N/V$ is often referred to as the 'Scorer parameter' If we imagine a two layer atmosphere with the upper layer having a larger value of $l_s$ than the lower layer, then it may happen that, for a given horizontal wave number k, the vertical wavenumber is imaginary in the upper layer and real in the lower layer. In such a case the wave is reflected at the interface and energy becomes trapped in the lower layer. This phenomenon gives rise to lee waves (see Scorer 1949). It is evident that such trapped waves are only possible if the atmosphere is assumed to be non-hydrostatice, since in a hydrostatic model the vertical wavenumber is real for any value of $l_s$ .

f) Characteristic features of mesoscale flow.

From the above discussion we may infer some general characteristics of mesoscale systems. These must be borne in mind when designing numerical models for predicting local weather

Spontaneous generation of discontinuities

Strong internal mixing layers

Strong interaction between 'physics' and 'dynamics'

Three dimensionality

Hydrostatic atmospheres more unstable than non-hydrostatic atmospheres

Interaction between mountains and synoptic scales

Wave drag and upward energy flux

Turbulence near critical levels

Trapped lee waves.

3. Initial data for mesoscale models

For forecasts of many mesoscale features for a short time ahead (0-6 hours) the most useful information will normally be supplied by a knowledge of present development, but this is not always readily available. Some aspects of the evolving situation can be deduced from movies of sequences of pictures obtained from Meteosat and from radar networks, but this type of information is limited to cloud and rainfall. Other information is supplied by hourly surface observations, aircraft winds, and pilot and radiosonde ascents at less frequent intervals. Even if good initial analyses were available their influence would be limited by diurnal modification of the atmospheric boundary layer and by snyoptic development. For example with a synoptic scale advective speed of $10ms^{-1}$, an air parcel would move across Britain in about 14 hours and consequently by 24 hours most of the observational information may be lost out of the down wind boundary of a limited area model. The corollary of this statement is that 24 hour mesoscale forecasts must be obtained from large scale and surface forcing alone. The extent to which this is possible is a matter for experiment, but the traditional practice of experienced forecasters implicitly assumes that is is feasible.

Organised mesoscale activity embedded in the synoptic scale flow (such as frontal rain bands) is unlikely to be quantitatively predictable unless it is detected in the initial data. However, there is some evidence that frontal precipitation cells are fairly long lived, and if their development time is short and the large scale parameters governing their growth are adequately represented, it may be possible for a numerical model to predict the character of the rainbelt but not the phase of the rainfall concentrations.

The problem of assimilating data into synoptic scale numerical models has been studied extensively. It has been recognised that if an isolated observation, which is inconsistent with the model forecast, is inserted it will give rise to gravity waves which rapidly disperse and dilute the information contained in the observation so that the forecast continues almost unaffected. Since in the atmosphere the wind and mass fields are in approximate geostrophic balance, observations which fail to satisfy this balance will initiate a geostrophic adjustment process. Theory suggests that on scales greater than $2\pi U/f \approx 600$ Km at mid latitudes ($U$ = wind speed $f$ = Coriolis parameter) the wind speed adjusts to the mass field, while on smaller scales the mass field adjusts to the wind field. The adjustment time is of the order $\pi/f$ (i.e. 6 - 12 hours for mid latitudes). This means that on large scales the insertion of

pressure information is likely to have the most lasting effect while at low latitudes and on small scales the most influential observations to assimilate are the wind data.

This behaviour cannot be extrapolated to the mesoscale. The problem of mesoscale data assimilation is not primarily one of geostrophic adjustment and there is very little information or understanding at present of what processes and what adjustment times are involved. Different mesoscale phenomena probably respond in different ways and are sensitive to different physical parameters. An unpublished experiment, performed in the U.K. Met. Office, illustrates the problem as it affects sea breezes. A non-hydrostatic mesoscale model was started at an initial data time of 0400Z and integrated to 1200Z for a day (14/6/73) on which good sea breezes were observed. Several integrations were then performed starting at 1200Z (when the sea breeze was well developed) with certain mesoscale meteorological fields replaced by values interpolated from a synoptic scale model. The same surface forcing scheme was used for all integrations. The idea behind the experiment was that fields taken from the mesoscale model were to be regarded as analyses deduced from a dense mesoscale observational network while those interpolated from the synoptic model were background values for which no observations were available. The different sets of initial data that were used are given in Table 1.

| Experiment | Data taken from mesoscale model | Data taken from 10-level model |
|---|---|---|
| 1 | Nil | Winds and temperatures at all levels |
| 2 | Winds at all levels | Temperatures at all levels. |
| 3 | Temperatures at all levels | Winds at all levels |
| 4 | Temperatures at lowest level only | Temperatures at all levels except lowest level and convective instability eliminated. Winds at all levels. |
| Control | Winds and temperatures at all levels | Nil |

TABLE 1

Comparing with the control experiment, the cases fell into two categories. Experiments 1 and 2 developed sea breezes which were about 2 hours behind those in the control in both intensity and position. Experiments 3 and 4 were almost identical to the control. This suggests that for sea breezes the winds adjust to the mass field (in complete contrast to geostrophic adjustment) and that the only relevant data required for sea breeze forecasts are details of the surface air temperatures (evidently the development of an elaborate wind analysis scheme is unnecessary for sea breeze forecasts). Clearly many additional experiments of this kind must be made before the sensitivity of forecasts to initial observations is understood.

The observations considered below should all be considered for use in a small scale 4 dimensional data assimilation scheme.

(i) Hourly surface and current weather observations

These can be subdivided into

(a) observations of temperature, humidity, pressure, pressure tendency and winds.

(b) observations of weather, visibility, cloud type and cloud base.

(i) (a) At present, this is the only source of reliable observations of the primary dynamical variables with a complete areal coverage. The fact that the observations are limited to the surface is a major deficiency, but if a sparse network of upper air observations ((ii), (vi)) can be used to provide the vertical detail, the surface observations might provide the horizontal detail required for a full three dimensional analysis. Since a poor analysis of the dynamical variables will produce a rapid degradation in the quality of the other fields (vertical velocity, humidity, and cloud), most effort should be put into the observations and analysis of wind, temperature and pressure. The best use of surface observations of these variables is the most urgent problem in mesoscale and small scale analysis.

(i) (b). These observations are similar in type to satellite (iv) and radar (v) observations in that they give qualitative information that is not easy to interpret in terms of the model fields. Observations of cloud type and base could be interpreted in terms of boundary layer structure and might be extremely useful, but the accuracy of cloud base estimates would have to be proved. A further use of these data would be to categorise air mass types and, by analysing boundaries between types, use this information to improve the horizontal extrapolation of data provided at a limited number of sites e.g. radio sondes (ii).

(ii) Radio sondes

The 12 hour interval between ascents and the spacing of radio sonde stations are designed to meet synoptic needs. Nevertheless, at present they give the only direct measurements of vertical structure and will be invaluable. Their use is well tried and the only major work required is to discover the extent to which the information they provide can be extrapolated in the horizontal, as described under (i) (a)

(iii) Pilot Balloons

For certain types of phenomena the wind field is likely to become increasingly important as the scale decreases. If this is the case, it will be important to obtain frequent direct and high density measurements of horizontal wind velocity. This might be provided by pilot balloon ascents, and if more frequent ascents were available (say 3 hourly), they would help resolve the diurnal variations of the boundary layer. High level observations are not required, so the balloons used need to reach an altitude of only about 4km.

(iv) Satellite observation

Satellite observations, particularly Meteosat, could be used to provide guidance for human intervention in the analysis, but any intervention in frequent mesoscale analysis is not likely to be as effective or practical as the present intervention in the operational synoptic procedures. Observations of cloud type and cloud top height could provide useful information about the boundary layer structure and as in (i) (b), about air mass type. Displacement velocities may be a source of information about wind velocities, but the results are not likely to be as useful in these latitudes as GOES winds in the tropics.

(v) Radar observations

Radar observations are of rainfall only and are limited by the range of the radar. Possibilities exist for interpreting rainfall observations in terms of ascent, and estimates of vertical velocity would be useful and important if they were reliable, and if the horizontal velocities are known reasonably accurately. If either of these conditions is not satisfied the dynamical development of the model forecast will rapidly alter the initial vertical motion field. Again, radar can be used to provide displacement velocities and the usefulness of these should be investigated. Winds derived by radar and by satellite might be combined and calibrated with conventionally determined winds to give additional information at a distance from sonde ascents. Empirically derived quantities (vorticity, divergence, deformation) might also be obtained from cloud and rainfall fields and subsequently used to modify wind fields.

(vi) ADSEL and ASDAR

Modern navigation systems have enabled the latest range of commercial aircraft to install automatic wind and temperature measuring devices. At present these quantities are recorded every 4 seconds but plans are being worked out to automatically access this information by satellite and by radar (ADSEL and ASDAR). These data may be divided into those obtained during cruising, and those obtained during ascent and descent. Jet aircraft do not cruise at heights less than 5km, so the first group are probably of limited use for surface weather forecasting. However, the data obtained during landing and take-off will be useful provided that manoeuvering and temperature lags do not degrade the observations too greatly.

(vii) Climatological observations

These could be used to study the spatial autocorrelations and provide a means for interpolating between synoptic observations. This information should improve the usefulness of observations for analyses, and provide corrections that can be applied to grid point forecasts before applying these to particular locations.

The observations discussed above fall into two categories.

A) Direct observations of primary variables (i(a), (ii), (iii), (vi) and

B) Observations, usually novel, of other variables (i) (b), (iv) (v)

For the most part, the observations in (B) must be interpreted, using rather tenuous arguments, in terms of fields that deviate rapidly from their initial values when the wind and temperature fields are in error. Before expending great effort in the use of novel arguments and observations, it is important to understand the processes and fields that control the dynamics of small scale systems, and thus to understand what observations are required for the production of a reliable forecast. In the interim it seems most likely that a better use of the surface observations (i) (a) and improved coverage of pilot balloon ascents will give the best results.

4. Hydrostatic Models

A large number of mesoscale phenomena are adequately described by hydrostatic dynamics. In these cases advantage can be taken of the greater simplicity and familiarity of hydrostatic models, which may simply be fine mesh versions of synoptic scale models. The majority of attempts at forecasting on small scales have used hydrostatic schemes (Anthes (1978), Pielke (1973) and several others). This section contains three contrasting examples. The first illustrates the effect of reducing the resolution in a limited area fine mesh model for a prediction of frontal rain. The second demonstrates the possibilities

of using a sub grid scale diagnostic model for predicting orographic rainfall, while the third shows that even some extreme conditions involving airflow over mountains are capable of being predicted by hydrostatic dynamics.

a) The effects of increased resolution on frontal rainfall forecasts.

Fine mesh limited area models have been used for some time for regional forecasts (for example Burridge and Gadd 1976). Realistic frontal rain belts are formed after an initial adjustment period (6 - 12 hours), despite the absence of detail in the initial data, although rainfall amounts are usually under forecast. The results of Hoskins (1972) (see Section 2a) suggest that the critical parameters for frontogenesis are associated with the relationship of the deformation field and the large scale temperature gradient.

Since the essence of a front is a discontinuity, it might be expected that an improved forecast would result if the resolution were reduced. However, it is not clear how great the improvement would be and whether it justifies the increased cost of doing the forecast.

A recent experiment performed by Bell (1978) was designed to test the influences of horizontal and vertical resolution on the development of fronts. The model used was a limited area $\sigma$ coordinate model which had boundary conditions supplied by a larger scale forecasting model.

The fine mesh model contained rainfall processes, convective adjustment and surface heat and momentum transfers. The finite difference scheme was similar to the split explicit scheme of Gadd (1978). The equations were split into an advective part and gravity wave adjustment part, with the adjustment part integrated over four short $\delta t$ time step for each time step $\Delta t$ of the advective part.

Three versions of the model were tested (Table 2)

| Model | Number of levels | level separation | Grid length |
|---|---|---|---|
| A | 9 | 0.1 | 100km |
| B | 18 | 0.05 | 100km |
| C | 9 | 0.1 | 50km |

TABLE 2

The results are illustrated in Figs. 10 and 11 .

They show that the effect on the pressure forecast of increasing the horizontal resolution is negligible, but the forecast with a 50km mesh has appreciably more rainfall than was obtained using 100km. The three main areas of precipitation are forecast to be 32.6mm, 18.4mm, and 19.6mm

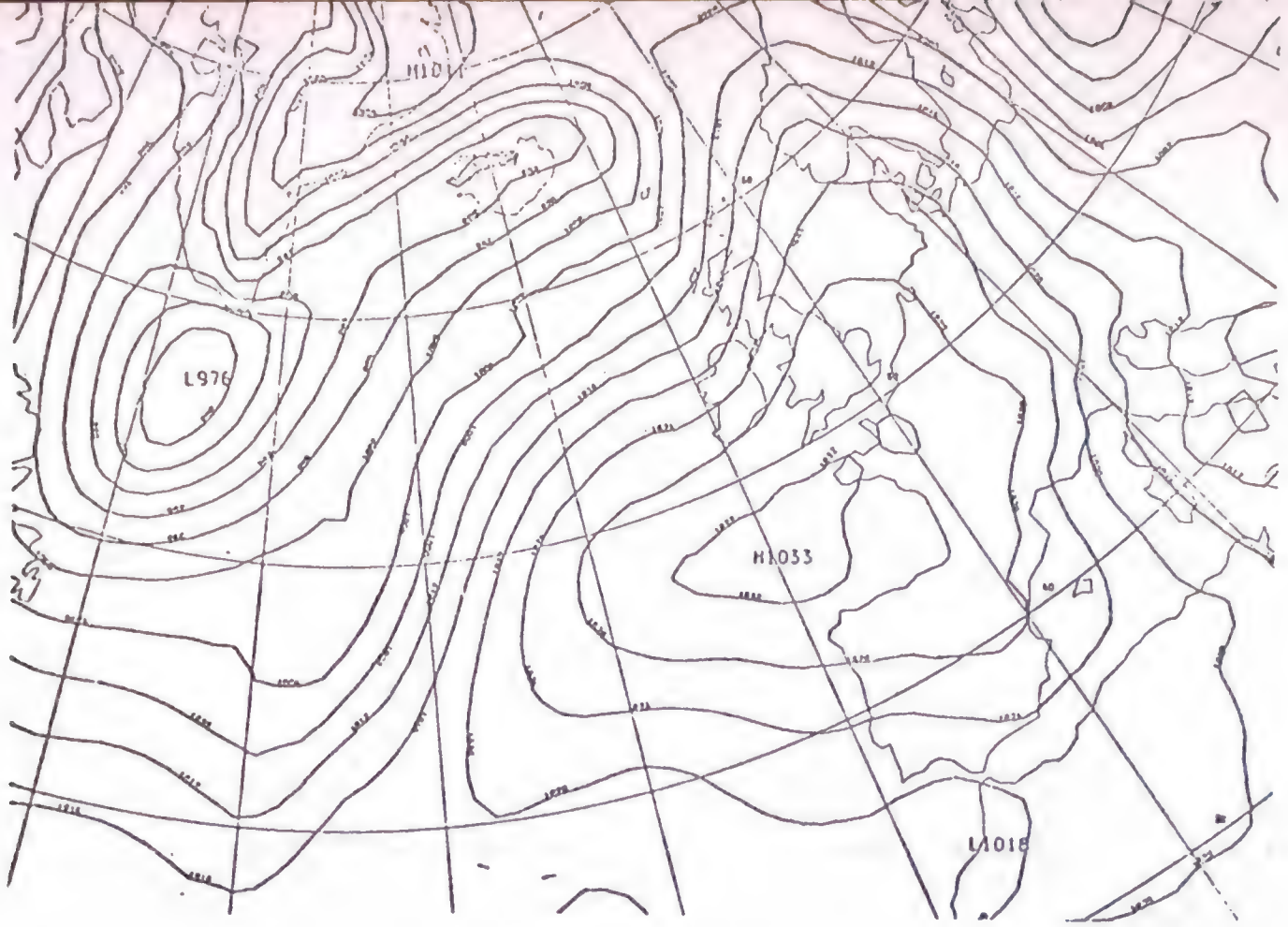


(a)

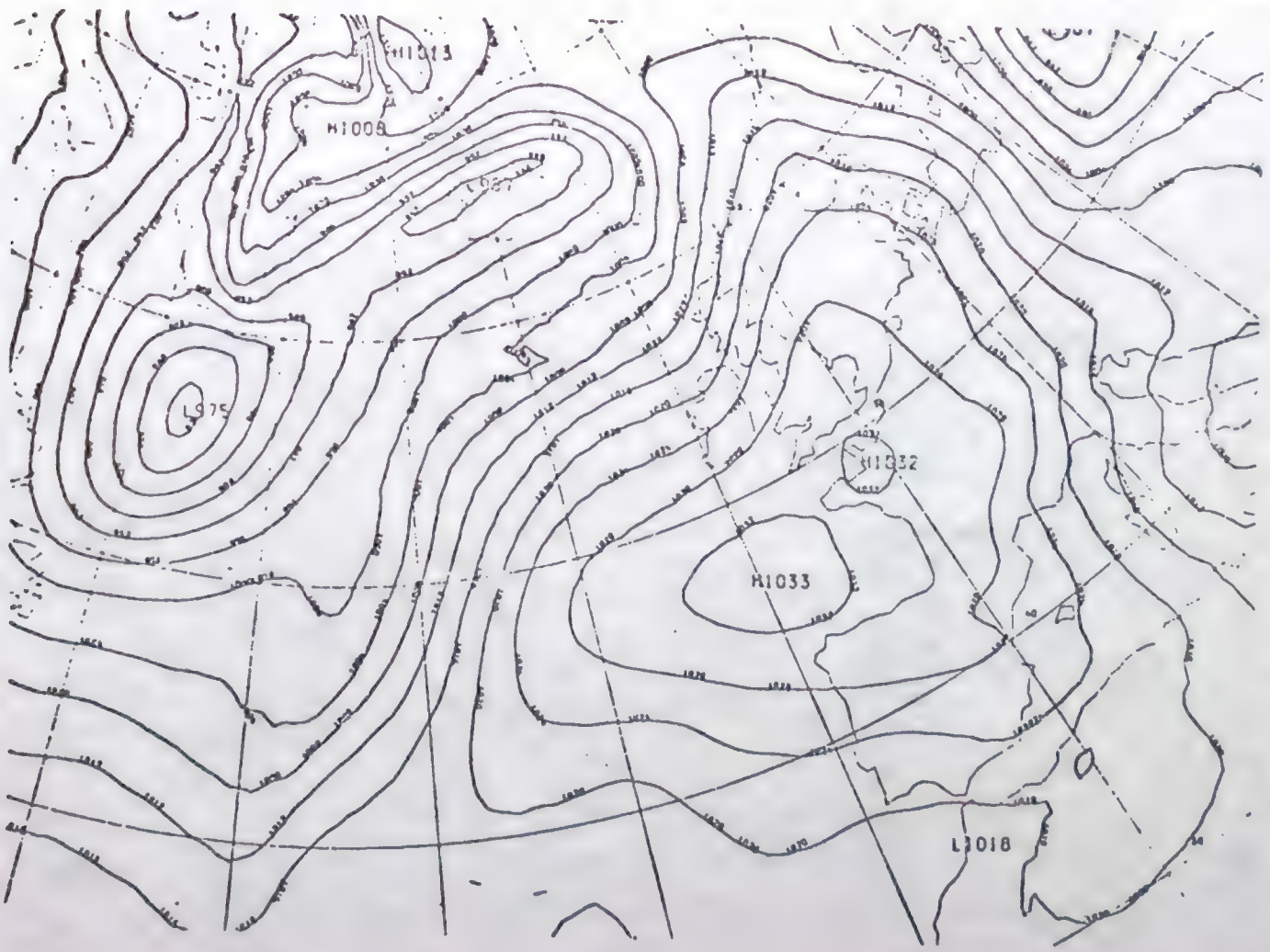


(b)

Fig.10 12 hour surface pressure forecasts with (a) 100km grid length and (b) 50km grid length (Bell 1978)

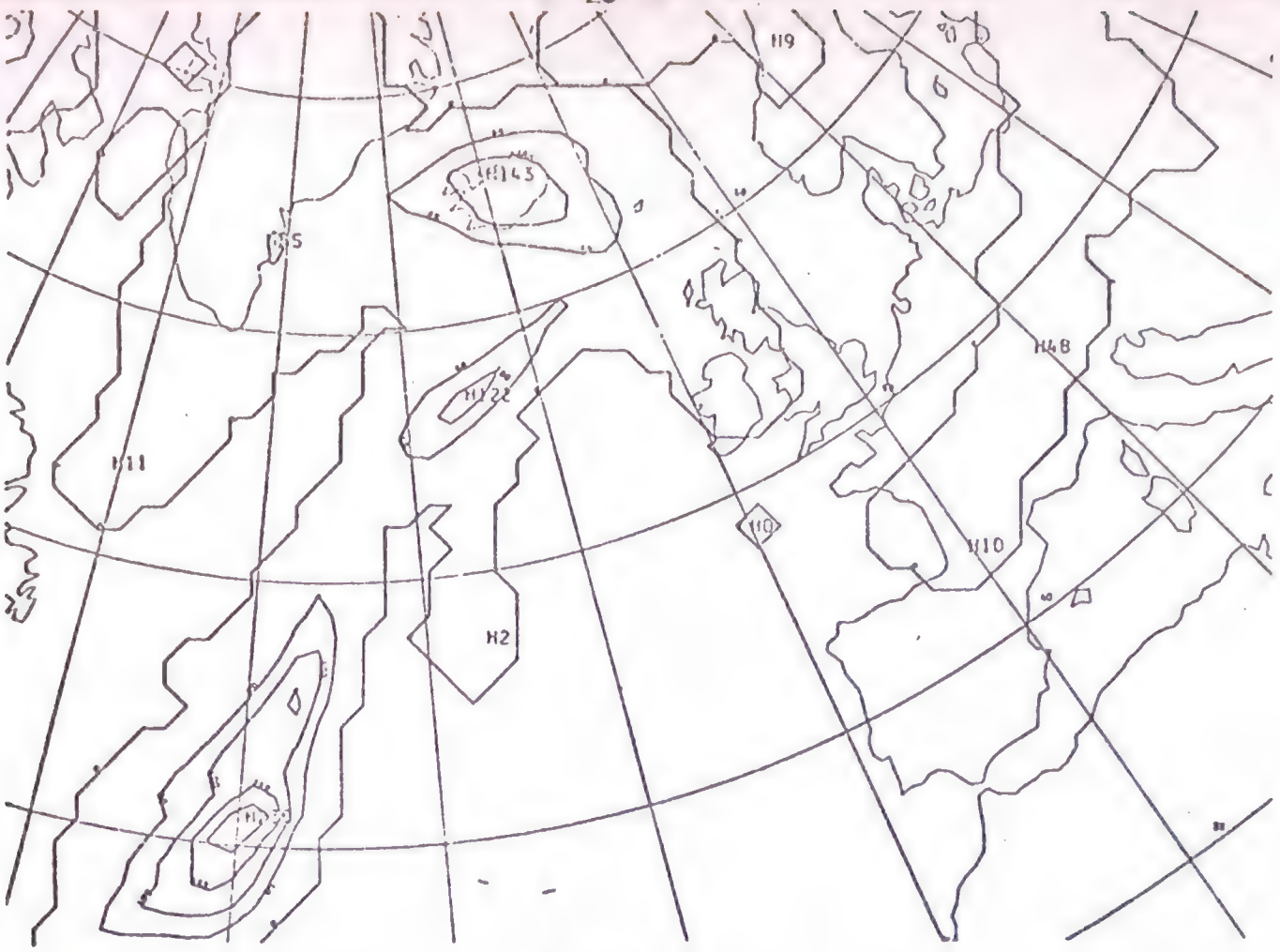


(a)

(b)

Fig.11 12 hour forecasts of accumulated rainfall with (a) 100km grid length and (b) 50km grid length (Bell 1978)

over 12 hours while 100km grid gave 23.6mm, 12.2mm and 14.3mm: - an increase of some 40%. The results confirm those of other investigations (Miyakoda and Rosati (1977), Shuman (1978), Phillips (1978)). It is also interesting to note the additional detail in the 50km forecast. One problem which may arise if the grid length is reduced too much is that over-vigorous convective cells may arise because of the sensitivity of hydrostatic models. Phillips has reported that in this case hydrostatic models may forecast spuriously large amounts of rain.

b) Orographic rainfall

It is well known that the observed accumulations of rainfall are closely related to the local orography. Current operational limited area fine mesh models (see Burridge and Gadd 1977) do not succeed in predicting sufficient orographic enhancement of the rain belts. One suggestion is that the airflow over the hills produces low level cloud. Pre-existing frontal rain produced from medium level cloud then falls through the low level cloud, and is enhanced by coalescence with the low level cloud droplets. (see Fig. 12)

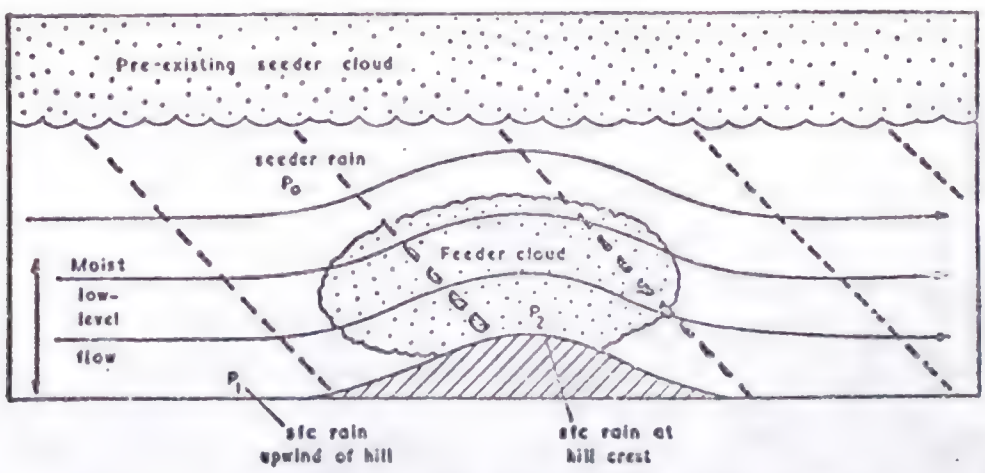


Conceptual model illustrating the orographic enhancement of rain (After Bergeron 1965).

**Fig. 12.**

If this is the case more detailed cloud physics is required than is present in most forecasting models. Bell (1978) has described a sub-gridscale model, containing sufficient physics to represent this process, and he has used it to attempt to forecast the local rainfall in Wales.

The model makes use of orography on a 3½km grid to predict local vertical velocities as a function of horizontal winds interpolated from a larger scale synoptic model with a grid length of 100km. The vertical velocity $\omega = \partial p/\partial t$ is given by

$$\omega = \omega_L + \omega_T$$

where $\omega_L$ is the vertical velocity as given from the synoptic scale model.

$$\omega_T = -F(p)\, \underline{V}_L \cdot \nabla H$$

where $\underline{V}_L$ is the large scale wind interpolated onto the fine mesh and H is the difference between the fine scale orographic height and the large scale orography. F is assumed to decrease linearly from one the surface to zero at 500mb. The rate of rainfall formed is given by

$$P_1 = -k_1 k_2\, \omega (\partial r_s / \partial p) \rho \Delta z$$

where $r_s$ is the saturated mixing ratio $\Delta z$ is the thickness of the layer, $k_1$ takes the value one for saturated ascent and zero otherwise, and $k_2$ depends on the length of time that the ascending air has been saturated. Precipitation falling into the next layer is enhanced by accretion of cloud water to give at total rainfall rate $P = P_1 + P_2$ , where $P_2$ is calculated from a formula used by Bador and Roach (1977). The model also includes schemes for representing evaporation and precipitation drift.

Bell used this technique in the form of a diagnostic local forecasting model, although another way it could be used is as a means of parameterising local rainfall in large scale models. Fig. 13 shows a plot of forecast error against observed rainfall and indicates that the underforecasting of the synoptic scale model for large rainfall rates has been corrected. Fig. 14 shows the observed rainfall and the local rainfall produced by Bell's model one one day in the test period. The amounts and positions of the maximum rainfall intensities have been well predicted.

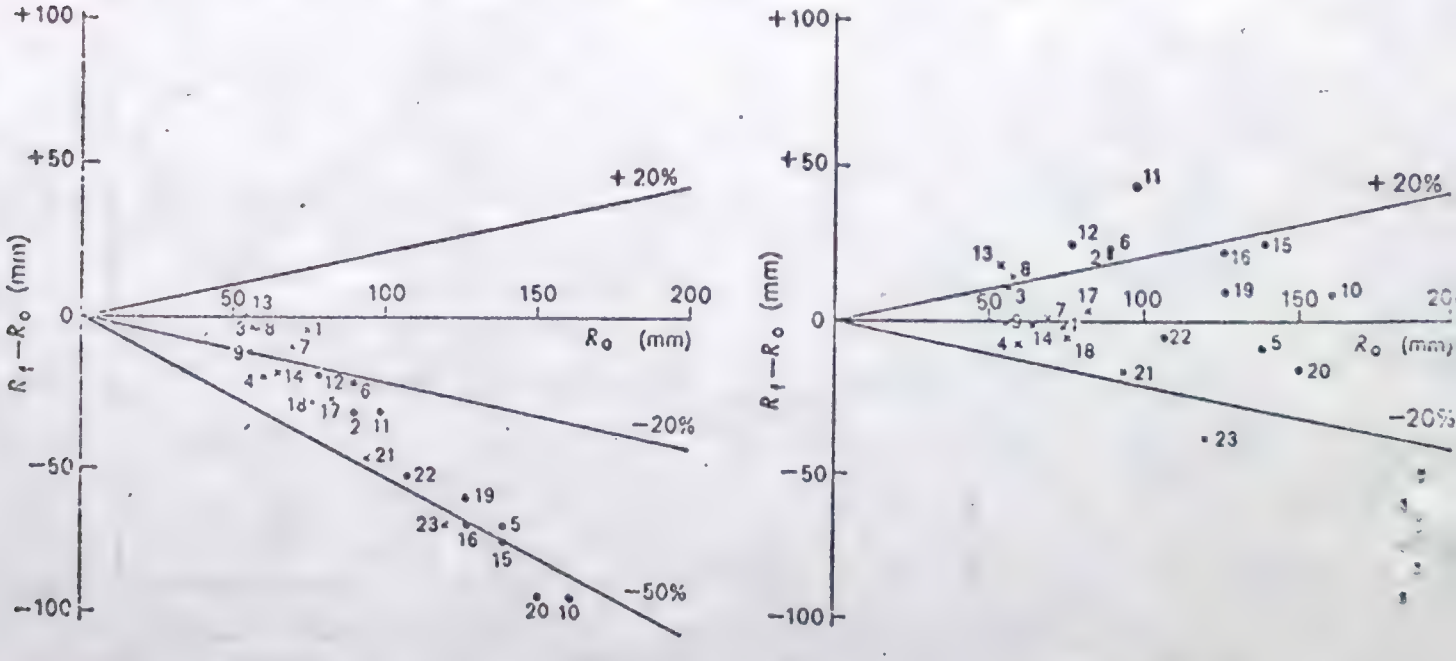


(a) 10-level model

(b) Orographic model

Fig. 13 —PLOT OF (FORECAST RAINFALL MINUS OBSERVED RAINFALL) AGAINST (OBSERVED RAINFALL) FOR TWO WEEK PERIOD

(a) compares results from 10-level model with observed rainfall.
(b) compares results from orographic model with observed rainfall.
O hilly areas X lowland areas
The straight lines show the bounds for forecast errors of 20% and 50% respectively.

Bell (1978)

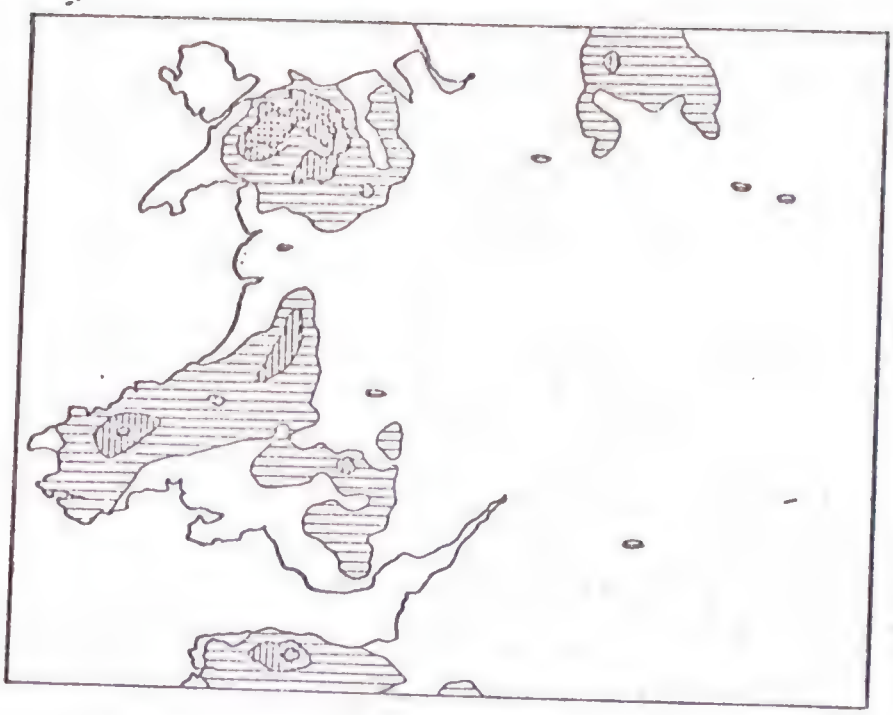

-RAINFALL ESTIMATED FROM RAIN-GAUGES FOR 14 OCTOBER 1976
Horizontal hatching indicates rainfall between 25 and 50 mm, vertical hatching rainfall between 50 and 75 mm, and cross-hatching rainfall in excess of 75 mm.

(Bell 1978)

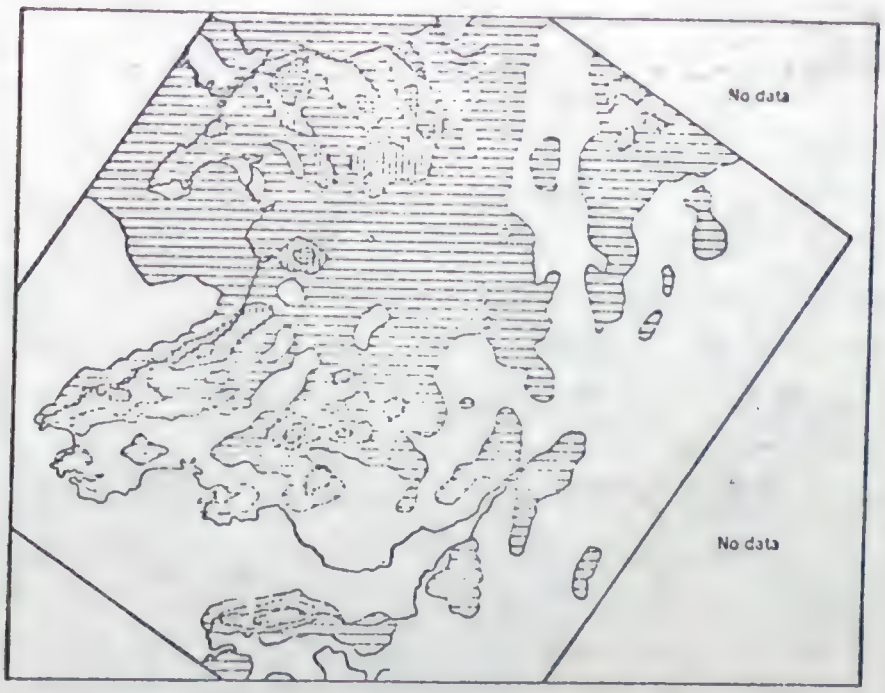


—RAINFALL FORECAST BY OROGRAPHIC MODEL ON 14 OCTOBER 1976
Horizontal hatching indicates rainfall between 25 and 50 mm, vertical hatching rainfall between 50 and 75 mm, and cross-hatching rainfall in excess of 75 mm.

(Bell 1978)

Fig. 14

c) Severe downslope winds and critical level absorption.

In a recent paper Klemp and Lilly (1978) have discussed the use of a two dimensional hydrostatic model to predict air flow over the Rockies on two occasions (11/1/72 and 17/2/70) with quite different flow characteristics. On the first of these days exceptionally strong surface winds were reported to the lee of the mountains with gusts up to $55ms^{-1}$. The second occasion did not have particularly strong surface winds, but there was a large amplitude wave near the tropopause with associated regions of severe turbulence.

The model equations used $\theta$ as a vertical coordinate and were integrated until a steady state was reached. Several preliminary integrations were performed in order to test different methods of specifying non relective upper boundary conditions which permitted wave energy to be radiated upwards. They found that if an artificial upper viscous layer were used, great care had to be exercised in ensuring that the value of the viscosity increased slowly with height to avoid reflections. For most of the integrations as many as 20 levels were required in this boundary zone to achieve acceptable results.

The equations were integrated using centred second order accurate difference schemes and the viscosity was set to zero in the 'real' part of the integration domain. A scheme to provide mixing when the Richardson number dropped below $\frac{1}{4}$ was also used. The case studies used initial and upwind data derived from a single radiosonde. Both cases were, to a large degree, well predicted. Strong surface winds in excess of $50ms^{-1}$ were produced in the down slope wind storm case (11/1/72)(see Fig.15) while in the second situation the large amplitude wave near the tropopause gave rise to a region where the horizontal wind dropped to zero suggesting the existence of a critical layer (Fig. 16 ). As test of the model's ability to cope with critical layer absorption, an integration using a wind profile linearly decreasing with height was performed. It was found that the Richardson number turbulence scheme was important in order to eliminate small vertical scales near the critical layer but that partial reflections caused by inadequate resolution in the vertical as the vertical wave number tended to zero at the critical level made the momentum flux predictions unreliable.

5. Non hydrostatic models

The full non-hydrostatic equations support the existence of high frequency acoustic waves as well as gravity and Rossby waves. For reasons of stability, numerical models with explicit integration schemes use a time step which shorter than the shortest period wave capable of being

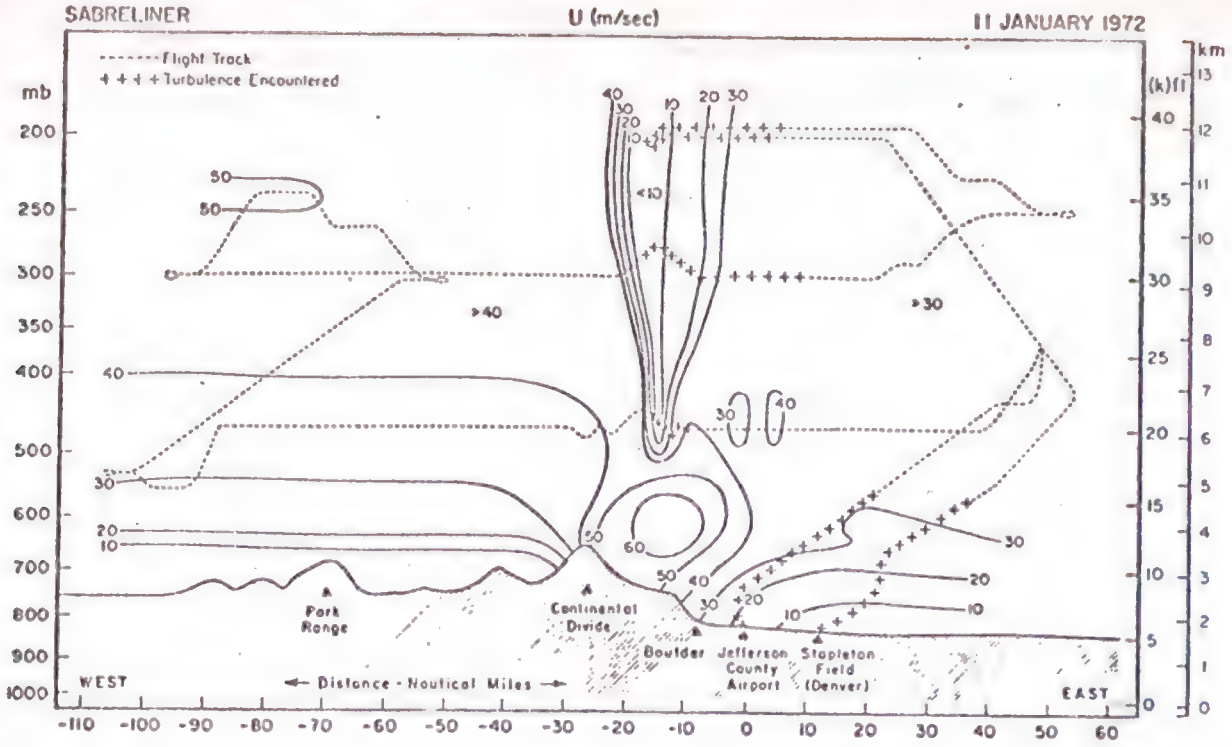


(a)

Fig.15 (a) observed and (b) predicted wind speeds ($msec^{-1}$) for 11 January 1972 (Klemp and Lilly 1978)

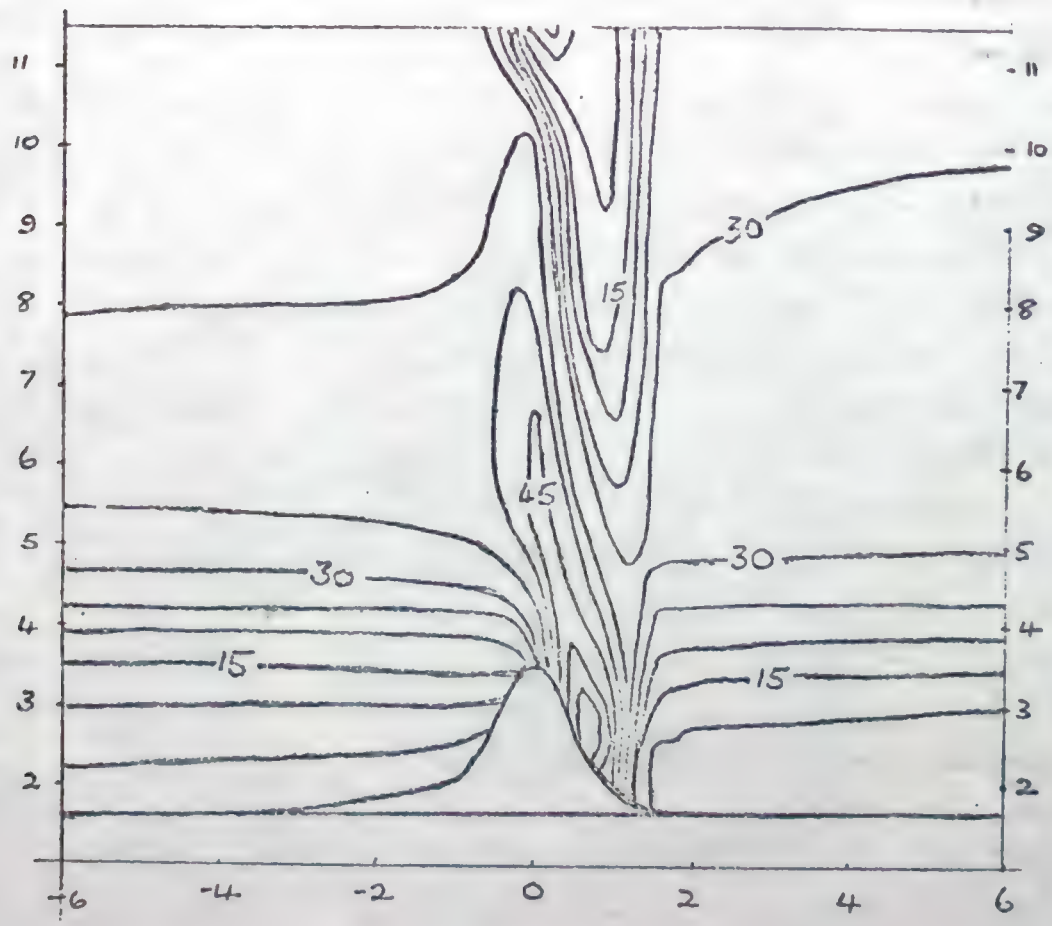


(b)

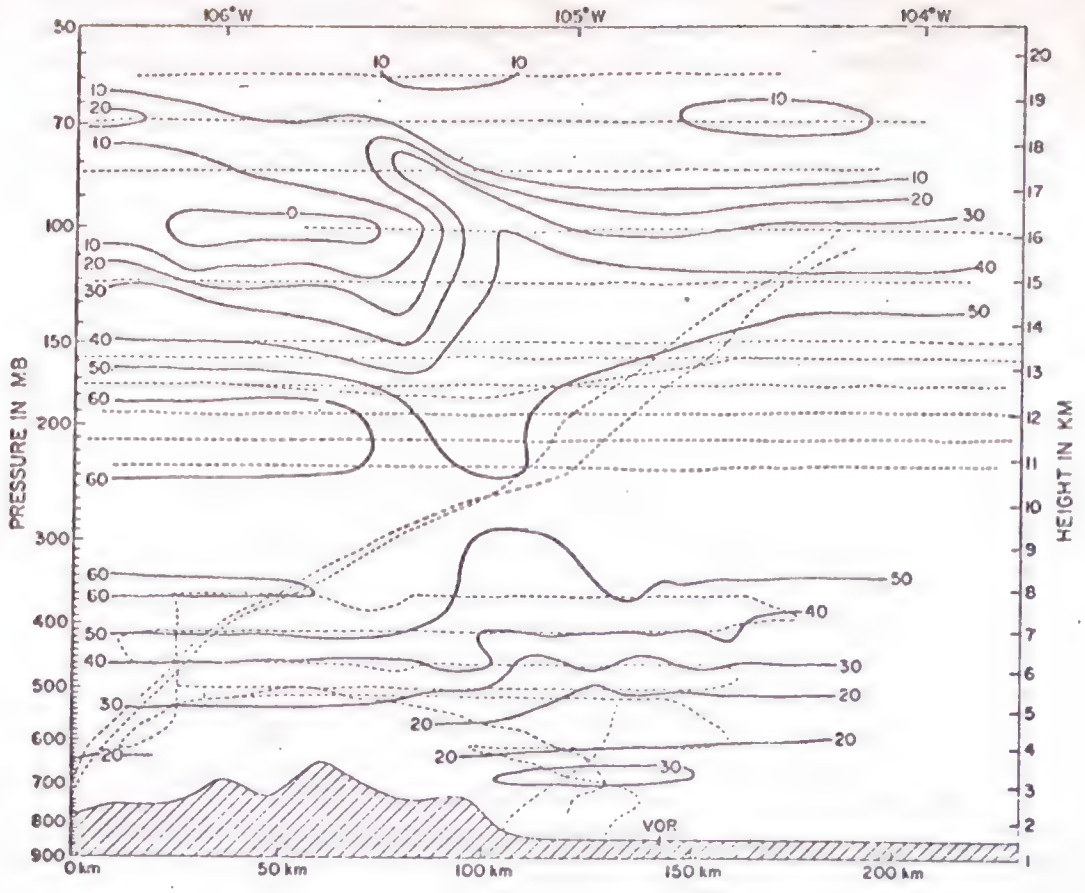


(a)

Fig.16 (a) observed and (b) predicted wind speeds ($msec^{-1}$) for 17 Feb. 1970 (Klemp and Lilly 1978)

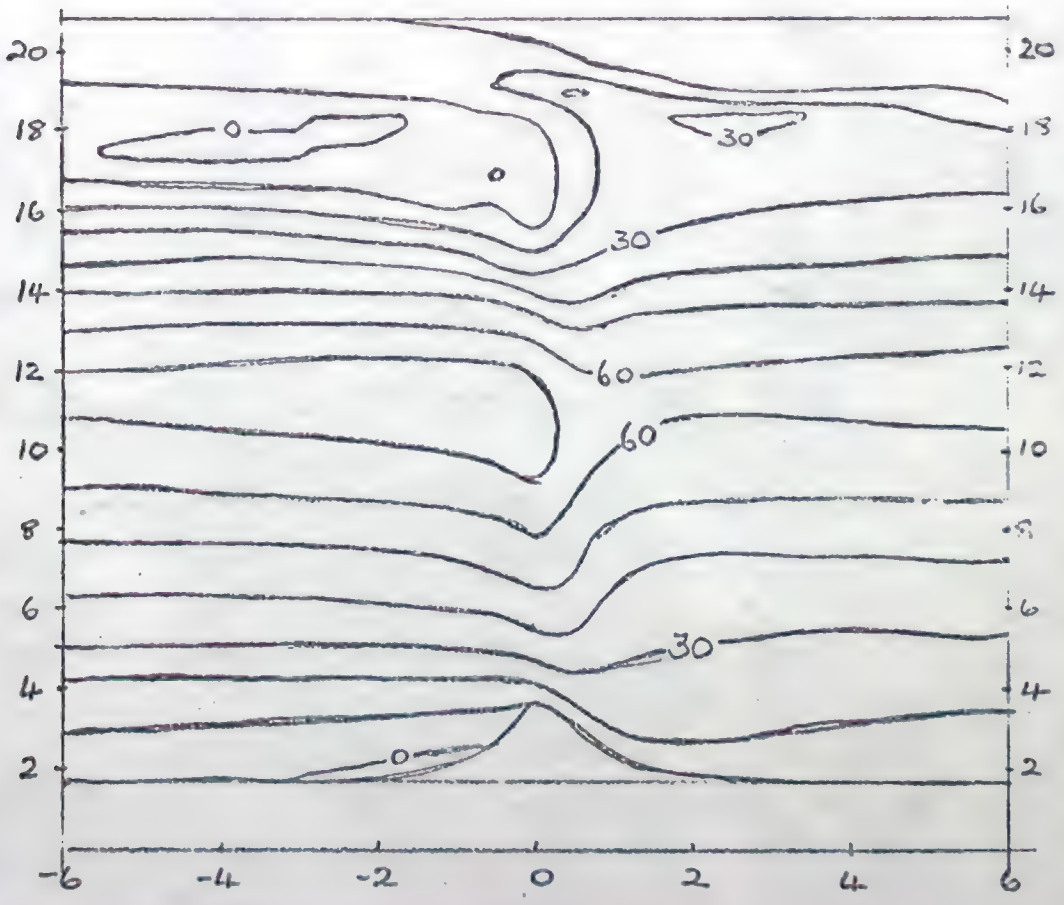

(b)

represented by the system. When vertically propagating sound waves are present this imposes severe computational penalties. Several ways have been devised in order to circumvent the problem. These techniques are based either on introducing some approximations into the equations or on using special numerical techniques.

a) The quasi-hydrostatic approximation

A model to predict the evolution of convective storms was developed by Miller and Pearce (1974). They used the complete equations, except that an approximation was introduced into the vertical equation of motion

$$\frac{Dw}{Dt} + g + \frac{1}{\rho}\frac{\partial p}{\partial z} = 0 \qquad (12)$$

by rewriting it in the form

$$-\rho\frac{\partial h}{\partial p} = \frac{1}{g}\left(1 + \frac{1}{g}\frac{Dw}{Dt}\right)^{-1} \approx \frac{1}{g}\left(1 - \frac{1}{g}\frac{Dw}{Dt}\right)$$

an approximation which is valid for $g^{-1}\, Dw/Dt \ll 1$

The hydrostatic pressure may then be introduced as the vertical coordinate instead of z to give

$$\frac{\partial u}{\partial t} + \omega\frac{\partial u}{\partial p} - v\zeta + \frac{\partial \psi}{\partial x} = F_x \qquad (13)$$

$$\zeta = \frac{\partial v}{\partial x} - \frac{\partial u}{\partial y} + f$$

$$\frac{\partial v}{\partial t} + \omega\frac{\partial v}{\partial p} + u\zeta + \frac{\partial \psi}{\partial y} = F_y \qquad (14)$$

$$\frac{\partial \omega}{\partial t} + \underline{v}\cdot\nabla\omega + \omega\rho_s\frac{\partial}{\partial p}\left(\frac{\omega}{\rho_s}\right) + \rho_s g^2\frac{\theta'}{\theta_s} + g^2\rho_s^2\frac{\partial h'}{\partial p} = 0 \qquad (15)$$

$$\frac{\partial u}{\partial x} + \frac{\partial v}{\partial y} + \frac{\partial \omega}{\partial p} = 0 \qquad (16)$$

$$\frac{\partial \Theta}{\partial t} + \frac{\partial}{\partial x}(u\theta) + \frac{\partial}{\partial y}(v\theta) + \frac{\partial}{\partial \omega}(\omega\theta) = q \qquad (17)$$

where $\rho_s$ is the density of the standard atmosphere, $h'$ and $\theta'$ deviations of the height and potential temperature from their standard values, and $\psi = gh' + \frac{1}{2}(u^2 + v^2)$.

In many ways this technique is the hydrostatic analogue of the method of deriving the quasi-geostrophic equations. The pressure is assumed to be hydrostatic everywhere except in the vertical equation of motion. In solving equations ( 13 ) - ( 17 ), the continuity equation is satisfied by solving

$$\frac{\partial}{\partial t}\left(\frac{\partial u}{\partial x} + \frac{\partial v}{\partial y} + \frac{\partial \omega}{\partial p}\right) = 0$$

This leads to a 2nd order partial differential equation for the height

$$\frac{\partial^2 h'}{\partial x^2} + \frac{\partial^2 h'}{\partial y^2} + g^2 \frac{\partial}{\partial p}\left(\rho_s^2 \frac{\partial h'}{\partial p}\right) = F(x, y, z)$$

Miller has shown that the approximation eliminates sound waves, but retains both the Lamb wave and the non-hydrostatic behaviour of gravity waves.

b) Split partially implicit finite difference scheme

In a recent paper Klemp (1978) has described a method of integrating the full non-hydrostatic compressible equations using a special finite difference scheme. Writing the equations in the form

$$\frac{D}{Dt}\underline{v} + f\,\underline{k}\times\underline{v} - g\frac{\theta'}{\theta_s}\underline{k} + c_p\theta\,\nabla\Pi = \underline{F}$$

where $\Pi = \left(\frac{p}{p_s}\right)^{R/c_p}$. A prognostic equation for $\Pi$ is obtained by writing

$$\frac{\partial \Pi}{\partial t} = \frac{\partial}{\partial t}\left(\frac{p}{p_s}\right)^{R/c_p} = \frac{\partial}{\partial t}\left(\frac{R\rho\theta}{p_s}\right)^{R/c_v}$$

and eliminating $\frac{\partial \rho}{\partial t}$ and $\frac{\partial \theta}{\partial t}$ by using the continuity equation

$$\frac{D\rho}{Dt} + \rho\,\nabla\cdot\underline{v} = 0$$

and the thermodynamic equation

$$\frac{D\theta}{Dt} = Q$$

this gives

$$\frac{D\Pi}{Dt} + \frac{c^2}{\rho c_p \theta^2}\nabla\cdot(\rho\theta\underline{v}) - \frac{R}{c_p}\Pi\,\nabla\cdot\underline{v} = \frac{c^2 Q}{c_p\theta^2}$$

where $c$ is the speed of sound.

The technique of solving the equations by finite differences is to separate those terms which are involved in sound wave propagation onto the left hand side of the equation leaving other terms on the right hand side.

$$\frac{\partial u}{\partial t} + c_p\theta_s\frac{\partial \Pi}{\partial x} = f_1 \qquad (18)$$

$$\frac{\partial v}{\partial t} + c_p\theta_s\frac{\partial \Pi}{\partial y} = f_2 \qquad (19)$$

$$\frac{\partial w}{\partial t} + c_p\theta_s\frac{\partial \Pi}{\partial z} = f_3 \qquad (20)$$

$$\frac{\partial \Pi}{\partial t} + \frac{c^2}{c_p\theta_s}\left(\frac{\partial u}{\partial x} + \frac{\partial v}{\partial y}\right) + \frac{c^2}{c_p\rho_s\theta_s}\frac{\partial}{\partial z}(\rho_s\theta_s w) = f_4 \qquad (21)$$

Since a centred time step is used, we require to step from $t-\Delta t$ to $t+\Delta t$. In order to maintain stability for sound waves this is accomplished by performing the operation in n short time steps of length $2\Delta t/n$. The right hand sides do not involve sound wave

propagation and are kept constant at their values at time level t.

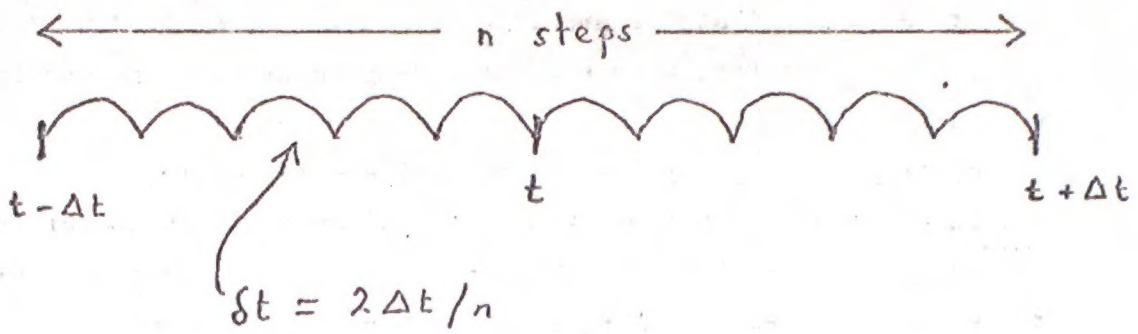


Since the vertical grid length is much smaller than the horizontal grid length the stability of this procedure requires a times step proportioned to $\Delta z/c$ . In order to increase this, Klemp uses an implicit finite difference scheme in the vertical. The stability criterion is then $\Delta t < n\Delta x / 2\sqrt{2}\, c$

c) Semi Implicit scheme

Tapp and White (1976) developed a semi-implicit scheme. Their basic organisation is similar to that of Klemp (1978) except that the left hand sides of equations ( 18 ) - ( 21 ) are all represented implicitly with a finite difference scheme of the form

$$\frac{u(t+\Delta t) - u(t-\Delta t)}{2\Delta t} + \frac{c_p \theta_s}{2}\left[\frac{\partial \pi}{\partial x}(t+\Delta t) + \frac{\partial \pi}{\partial x}(t-\Delta t)\right] = f,$$

The equation for $\overline{\pi}$ then takes the form (after eliminating variables other than $\overline{\pi}$)

$$\frac{\partial^2 \overline{\pi}}{\partial x^2} + \frac{\partial^2 \overline{\pi}}{\partial y^2} + \left[\frac{\partial^2}{\partial z^2} - \frac{g}{c^2}\frac{\partial}{\partial z} - \frac{1}{c^2 \Delta t^2}\right]\overline{\pi} = F$$

The stability of this scheme does not depend on the speed of sound, but the time step must satisfy a condition of the form

$$\Delta t < \min\left(1/N\ ,\ \Delta x/\sqrt{2}\,U\ ,\ \Delta z/W\right)$$

where N is the Brunt Vaissala frequency, U is wind speed and W is the vertical velocity. The larger time steps which can be used compared to

the split partially implicit scheme are offset by additional computation involved in solving a three dimensional partial differential equation.

Each of these three schemes has been used successfully in a number of experimental simulations. The quasi hydrostatic equations have been used for cumulonimbus simulations by Miller and Pearce (1974) and Miller (1978). The partially implicit scheme has been used for the simulation of the splitting of convective storms by Klemp and Wilhelmson (1978) while the semi implicit technique has been used for forecasts of actual sea breezes, and for simulations of cumulus and lee wave dynamics (Carpenter, 1978). It is too early to say if one of the schemes has some particular advantage over the others.

REFERENCES


Anthes, R.A and Warner, T.T 1978 'The development of mesoscale models suitable for air pollution and other meso meteorological studies'. Unpublished report. Dep. Meteorology Penn State Univ.

Bell, R.S 1978 'A versatile limited area sigma coordinate model - preliminary results showing the effect on forecast rainfall of changing the resolution'. Unpublished report Met011 Tech.Note No.109 UK Met.Office Bracknell.

Bell, R.S 1978 'The forecasting of orographically enhanced rainfall accumulations using 10 level model data'. Met.Mag 107 p 113.

Benjamin, T.B 1968 'Gravity currents and related phenomena' J.Fluid Mech. 31 (2) p 209.

Bergeron, T 1965 'On the low level redistribution of atmospheric water caused by orography'. Suppl. Proc.Int.Conf.Cloud Phys. Tokyo May 1965 p 96.

Booker, J.R and Bretherton,F.P 1967 'The critical layer for internal gravity waves in a shear flow'. J.Fluid Mech 27 p 513.

Browning, K.A and Ludlam F.H 1962 'Airflow in convective storms'. Quart.J.R. Met.Soc. 88 p 117.

Burridge, D.M. and Gadd, A.J. 1976 'The Meteorological Office operational 10-level model (Dec.1975)' Met.Office Sci.Paper 34.

Eckart, C 1960 'Hydrodynamics of Oceans and Atmospheres'. Pergamon Press.

Eliassen, A 1973 'Airflow over mountains' Report UNESCO Summer School on Mesoscale meteorology. Nat.Res.Council Italy p53.

Gadd, A.J. 1978 'A split explicit integration scheme for numerical weather prediction'. Quart.J.R.Met.Soc. 104 p569.

Hoskins, B.J 1971 'Atmospheric frontogenesis models: some solutions'. Quart.J.R.Met.Soc. 97 p139.

Carpenter, K.M. 1978 'An experimental forecast using a non-hydrostatic meso-scale model'. Unpublished report Met011 Tech.Note No.106 UK Met.Office Bracknell.

| | | |
|---|---|---|
| Klemp, J.B | 1978 | 'A splitting procedure for numerical solution of the compressible equations of motion' Unpublished paper. |
| Klemp, J.B and Lilly, D | 1978 | 'A numerical simulation of hydrostatic mountain waves'. J.Atmos.Sci.35 p78. |
| Klemp, J.B and Wilhelmson, R.B. | 1978 | 'The simulation of three-dimensional convective storm dynamics'. J.Atmos.Sci.35 p1070. |
| Miller, M.J. and Pearce R.P. | 1974 | 'A three dimensional primitive equation model of cumulonimbus convection'. Quart J.R.Met.Soc.100 p133 |
| Miller, M.J. | 1978 | 'The Hampstead Storm; a numerical simulation of a quasi stationary cumulonimbus' Quart J.R.Met.Soc. 104 p35. |
| Miyakoda, K and Rosati, A. | 1977 | 'One way nested grid models, the interface conditions and numerical accuracy'. Mon.Weath.Rev.105 p1092. |
| Moncrieff, M.W | 1978 | 'The dynamical structure of two dimensional steady convection in constant vertical shear'. Quart J.R.Met.Soc. 104 p542. |
| Moncrieff, M.W and Green J.S.A | 1972 | 'The propagation and transfer properties of steady convective overturning in shear' Quart J.R.Met.Soc. 98 p336. |
| Pielke, R.A. | 1974 | 'A three dimensional numerical model of the sea breezes over South Florida' Mon.Weath.Rev. 102 p115. |
| Phillips, N.A | 1978 | 'A study of higher resolution numerical models'. Unpublished report NMC Washington. |
| Simpson, J.E. | 1969 | 'A comparison between laboratory and atmospheric density currents'. Quart J.R.Met.Soc. 95 p758. |
| Simpson, J.E, Mansfield, D.A and Milford, J.R | 1977 | 'Inland penetration of sea breeze fronts' Quart J.R.Met.Soc. 103 p47. |
| Shuman, F | 1978 | 'Numerical Weather Prediction' Bull.A.M.S. 59 No.3. |
| Tapp, M.J and White, P.W. | 1976 | 'A non hydrostatic mesoscale model' Quart J.R.Met.Soc. 102 p277 |